

A LOW RANK NEURAL REPRESENTATION OF ENTROPY SOLUTIONS

DONSUB RIM* AND GERRIT WELPER†

Abstract. We construct a new representation of entropy solutions to nonlinear scalar conservation laws with a smooth convex flux function in a single spatial dimension. The representation is a generalization of the method of characteristics and possesses a compositional form. While it is a nonlinear representation, the embedded dynamics of the solution in the time variable is linear. This representation is then discretized as a manifold of implicit neural representations where the feedforward neural network architecture has a low rank structure. Finally, we show that the low rank neural representation with a fixed number of layers and a small number of coefficients can approximate any entropy solution regardless of the complexity of the shock topology, while retaining the linearity of the embedded dynamics.

Key words. neural networks, low rank neural representation, reduced order models, dimensionality reduction, hyperbolic conservation laws

AMS subject classifications. 68T07, 41A46, 41A25, 65N15, 35L65

1 Introduction Current state-of-the-art numerical algorithms simulating realistic fluid dynamics, even when run on the best hardware available today, are not real time. One proposed strategy in accelerating these solvers is to seek approximations of solutions to partial differential equations (PDEs) with small degrees of freedom. A class of such approximations called *reduced models* have been successfully applied for solutions to certain parametrized PDEs [14, 38].

The reduced models are commonly constructed as linear low-dimensional approximations written as a superposition of a few basis functions, and we will refer to such models as *classical reduced models*. When such an approximation to the solution to a time-dependent problem is possible, the computational complexity required to evolve the solution forward in time often scales with the number of the basis functions [37]. For example, if standard numerical algorithms such as finite difference methods require polynomial in N complexity to compute one forward time step according to the PDE, where N is the number of finite difference grid points, a reduced model using $\log N$ basis functions would instead require the reduced polylogarithmic complexity in N to do so, allowing the simulations to run faster than real time. This difference in the reduced complexity is a key desired feature in reduced models.

The limitations of classical reduced models are readily seen when one attempts to produce one for the simplest of hyperbolic problems, even the advection equation [74, 16]. The cause is the slow decay rate of the Kolmogorov width [64] of the solution manifold; its lower bounds imply that there cannot be a small set of reduced basis functions whose superpositions can approximate the solution uniformly well [83, 60, 31]. More generally, non-classical reduced models are also not completely immune from such lower bounds; slow decay can be established even for nonlinear benchmarks such as the stable width and entropy for high-dimensional parametric transport equations [15, 73]. Also relevant in this context are studies of stability of classical reduced models [32, 58, 21, 1].

*Department of Mathematics, Washington University in St. Louis, St. Louis, MO 63130 (rim@wustl.edu)

†Department of Mathematics, University of Central Florida, Orlando, FL 32816 (gerrit.welper@ucf.edu)

Various attempts were made to obtain the reduced complexity for convection-dominated problems by incorporating the structure of the transport. To provide a possibly incomplete list of proposed approaches that are the most relevant to this work: template-fitting [74], method of freezing [4, 59], shock reconstruction [16], approximated Lax-Pairs [28], advection modes [40], transported snapshot interpolation (TSI) [83], shifted proper orthogonal decomposition (sPOD) [67], calibrated manifolds [9], Lagrangian basis method [54], transport reversal [70], registration methods [78], Wasserstein barycenters [24] or quadratic manifolds [26]. Some of these proposed methods can be viewed as dynamical low-rank approximations [43, 75].

However, relatively few methods we encountered [56, 79, 71] have demonstrated (1) it can be deployed in a numerical scheme to solve the PDE using the approximation (e.g. in Galerkin systems), and (2) has an online complexity matching that of classical reduced models. These works exploit a nonlinear model that composes two superpositions of a few basis functions. We will call the nonlinear class of reduced models that can be represented in compositional forms satisfying the two criteria *complexity-separated compositional reduced models*, or simply *compositional reduced models*.

The compositional reduced models, while achieving the two properties required of classical reduced models, have not yet demonstrated an ability to handle shock propagation in their full generality; they were tested in restricted settings without shock interaction. This is a serious limitation, since for many PDEs arising from fluid dynamics, shock formation and collision are defining features. For example, a typical entropy solution to the Burgers' equation is shown in Fig. 1.1. Shocks can form at various times, travel at varying speeds, and merge; new techniques are required to handle these challenges. For example, a computational approach called Front Transport Reduction (FTR) employs level sets to represent the changes in the shock topology [44].

The dearth of progress invites the question: What is the essential obstacle that prevents the handling of shocks for the compositional models? Part of the answer lies in the fact that while it is clear that the characteristic curves can be approximated well by a few basis functions in convective problems when, for example, the velocity is smooth, it is not at all clear what low-dimensional structure can be exploited in the presence of various shock configurations.

In another line of approach, there have been attempts to leverage deep learning models to overcome the difficulty [34, 41, 53, 36, 82, 29, 48, 66, 54, 25, 55, 2], but whether one can devise deep learning models that can be evolved according to the PDE with the reduced complexity remains an open problem. The currently existing models do not achieve the complexity found in successful classical reduced models [42]. Given the compositional models studied in the past, and given how the deep learning models are defined with layers of compositions, it is natural to ask if there is a variant of the standard feedforward architecture that can connect them.

There are previous theoretical results relating transport equations, reduced models, and neural networks, in a broad sense. An approximation of parametric linear transport equations was derived in the setting of smooth convective fields [47] by approximating the initial condition and the characteristic curves [84, 63]. Neural networks were shown to be capable of emulating the approximations of reduced basis methods [27, 46]. A more recent result [20] showed various estimates using the notion

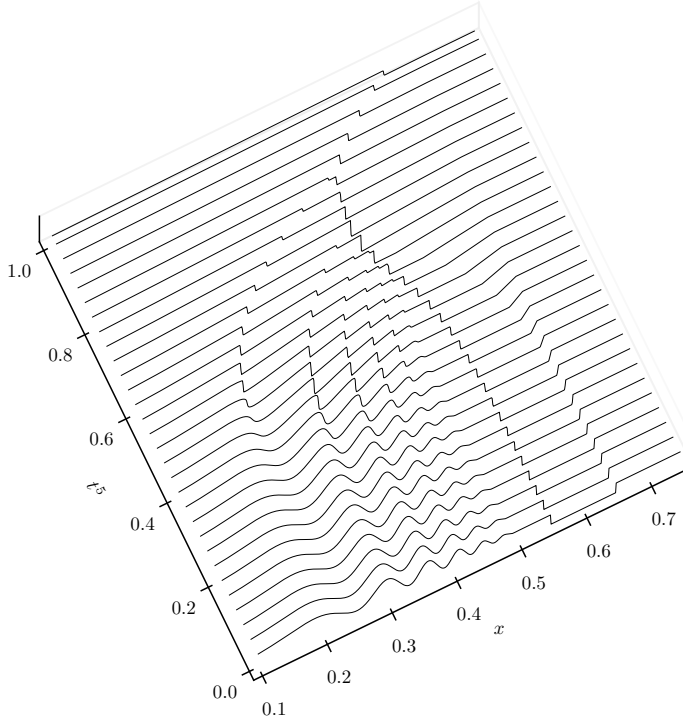


Fig. 1.1: An example of solution to the Burgers' equation. Time variable has been rescaled to better show details.

of *compositional sparsity*; e.g. when the high-dimensional parametric convection field has an affine decomposition, it was shown that there is a neural network approximation whose number of weight parameters depend linearly on the affine dimension.

In this work, we show one can exploit an inherent nonlinear low-dimensional structure in the entropy solution by repeated compositions, and present a theoretical construction in the form of a family of feedforward deep neural networks.

Neural networks that take spatial-temporal inputs are referred to as implicit neural representations (INRs) in deep learning or computer vision literature (e.g. [62, 77]); we follow suit and refer to our neural networks as INRs. Our construction can be viewed as a continuously parametrized family of INRs whose weight parameters are constrained to belong to a fixed low-dimensional linear space, and has the following desirable properties: (1) The construction is a direct generalization of the previous classical and compositional models, (2) the construction can approximate entropy solutions to nonlinear scalar conservation laws with arbitrarily many shocks and their interactions without an increase in the reduced dimensionality, and (3) the embedded temporal dynamics in the weights and biases of the INR is linear.

The first property is a key contribution of this work, showing that the previous compositional model that achieves online-offline decomposition [71] can be expressed

as 2-layer INR of this form, making the deeper analogue also a promising candidate model for achieving the reduced complexity.

The third property has important practical implications: Despite the involved spatial approximation, the temporal dependence of the weight parameters is linear. This suggests that this model has the potential to approximate complicated solutions while maintaining regular dependence on time. Such a feature would enable one to computationally integrate the representation in time, regardless of the lack of regularity in the spatial variable due to shocks. We briefly mention here a close relation between regular-in-time approximation introduced here and classical numerical methods exploiting similar properties, e.g. Large Time Step methods [49] or Averaged Multivalued Solutions [8]: These methods exploit the fact that classical characteristic curves are regular in time, that is, they are straight lines. These methods propagate the characteristics for longer durations than permitted by the Courant-Friedrichs-Lowy condition and then modify them to ensure proper shock propagation. We closely follow this principle of time-regular characteristic evolution with minimal modification. In contrast, standard finite-volume methods alter the characteristic curves at each time step and do not preserve their straightness or temporal regularity [50].

Another benefit of the temporal linearity is the favorable space-time approximation rates for entropy solutions in single spatial dimension, which are necessarily of bounded variation. Classical approximation methods require $\mathcal{O}(\epsilon^{-2})$ degrees of freedom to achieve L_1 error ϵ for such functions. In contrast, our results rely on the regularity of input data and the flux function, but not on specialized regularity classes such as cartoon-like functions [63, 5, 22, 52, 3]. That is, the input data consisting of initial value and the nonlinear flux function are single dimensional and can be approximated with only $\mathcal{O}(\epsilon^{-1})$ degrees of freedom. While the maximum width of our networks matches the degrees of freedom of classical method, we only require $\mathcal{O}(\epsilon^{-1})$ trainable weights due to the specialized architecture, and it is also possible to achieve $\mathcal{O}(1)$ evaluation time per point on a space-time grid.

We note an earlier work using reduced deep networks (RDNs) to approximate solutions to nonlinear wave problems [72], but the approximation here is an improvement in two important aspects: (1) In the earlier work, a bisection algorithm was implemented within the architecture using the feedforward layers which increased the number of requisite layers depending on the desired accuracy, and we avoid this here and the accuracy depends primarily on the width, and (2) The number of reduced dimensions do not depend on the number of shocks. As only speculated therein, this work illustrates a more concrete evidence of a new kind of depth separation, one that involves dimensionality reduction for deeper neural networks.

More recently, a continuously parametrized family of INRs was successfully used in the Physics-Informed Neural Networks (PINNs) framework [65, 10, 17], and exhibited improved convergence behaviors for solving PDEs that were challenging for the original PINNs [45, 13]. This general approach was referred to as Low-Rank PINNs (LR-PINNs).

Our construction here is a similarly parametrized family of INRs with low-rank architecture we call the Low-Rank Neural Representation (LRNR). We use the term LRNR to distinguish the technical definition of the architecture alone, as separate from the machine learning context, and to contrast with RDNs [72] which took on a different approach to approximating the weak solution. Readers familiar with the

LR-PINNs may view LRNR as a version of the architecture used in Low-Rank PINNs [13], keeping in mind that the time variable is treated as a parameter here rather than an input.

The trained LRNRs can serve as a reduced model approximation of the family of solutions to the parametrized PDEs: A rapid approximation is achieved due to the small number of degrees of freedom, much like the rapid computations performed during the online phase for classical reduced models. Moreover, it is not difficult to see that a reduction in online complexity can be achieved by utilizing the low rank structure in the weights and biases¹ much like the classical reduced models [38]. This is a property LRNR inherits by being a direct generalization of the compositional reduced model utilizing transported subspaces [71].

Due to the compositional structure, a connection can be made to the optimal transport problem that is associated with conservation laws [6, 24, 71]. Here, we depart from that connection and achieve an efficient representation of characteristic curves arising from nonlinear conservation laws without relying on optimal transportation.

Organization of the Paper The subject of this paper spans three different mathematical topics: The PDE theory of scalar conservation laws, reduced models, and neural networks. This paper is organized to cover all three aspects while aiming to keep each section as self-contained as possible.

- *Section 2.* This section introduces new representation of the entropy solutions. The PDE theoretical presentation is self-contained and covers the entropy solution in its full generality; that is, solutions with arbitrary shock and rarefaction waves.
- *Section 3.* A new neural network architecture called LRNR is introduced, inspired by the form of the new entropy solution representation from the previous section.
- *Section 4.* We discuss the close relation between a subclass of LRNRs and the compositional reduced model called transported subspaces. We develop an important technique called the inverse-bias trick, and we prove that classical solutions to scalar conservation laws can be approximated efficiently by a LRNR with two layers and rank three. This section also serves as an introduction of new ideas with relatively light technical details.
- *Section 5.* We develop a LRNR approximation to the entropy solutions by building on the new representation of the entropy solution developed in Section 2 and the inverse-bias trick from Sec. 4. We show that general entropy solutions can be approximated by a LRNR with five layers and rank two. This construction establishes a general low dimensional representation of the entropy solution, enabling an efficient representation of arbitrary shock wave interactions.

This paper introduces a substantial amount of new formulations and definitions. To aid the readers, the definitions and constructions are listed in a glossary in Appendix A. We will refer the reader to the glossary throughout the paper. Moreover, for brevity of presentation, the proofs of lemmas and theorems are postponed to Appendix B.

¹During the review of this work, a concrete result demonstrating this observation has appeared in [12].

2 A compositional form of entropy solutions In this section, we introduce the compositional forms of the entropy solution to nonlinear scalar conservation laws. We will first introduce the PDE and the generalized characteristics as well as the entropy solution. Then we introduce *rarefied characteristics*, which enables a representation of the entropy solution with a single composition without a separate description of the rarefaction fans. Finally, we derive yet another alternative representation of the entropy solution using *relief characteristics* which reveals a certain low rank structure in the entropy solution.

2.1 Entropy solutions In this section, we will describe the PDE that will be the focus of the paper.

For domains $\Omega_x, \Omega_t \subset \mathbb{R}$ let us denote by $C(\Omega_x)$ the space of continuous functions, by $C(\Omega_t; L^1(\Omega_x))$ space of continuous functions from Ω_t to $L^1(\Omega_x)$, by $P_0(\Omega_x)$ piecewise constant functions, and by $P_1(\Omega_x)$ piecewise linear functions.

Throughout, our spatial domain will be the unit interval $\Omega_x := (0, 1)$, and the temporal domain the interval $\Omega_t := (0, T)$ for some $T \in \mathbb{R}_+$. The space-time domain is denoted by $\Omega := \Omega_x \times \Omega_t$. We consider the scalar conservation law for $u : \Omega \rightarrow \mathbb{R}$,

$$(2.1) \quad \begin{cases} \partial_t u + \partial_x(F \circ u) = 0, & (x, t) \in \Omega, \\ u(\cdot, 0) = u_0, \\ u(0, \cdot) = u(1, \cdot) = 0, \end{cases}$$

where the initial value u_0 lies in

$$(2.2) \quad \mathcal{U} := \{v \in BV(\Omega_x) \mid v \text{ has compact support}\},$$

and we assume a smooth flux function $F \in C^\infty(\mathbb{R})$ that is strictly convex. We choose T to be small enough so that the zero boundary conditions are satisfied for all $t \in \Omega_t$.

For each $u_0 \in \mathcal{U}$, there exists Ω_t for which there is a solution $u \in C(\Omega_t; L^1(\Omega_x))$ such that $u(\cdot, t) \in \mathcal{U}$ for all $t \in \Omega_t$. See standard texts, for example [76, 50, 19], for proofs and references as well as numerical approximations.

It is possible to construct a convergent sequence to the solution u by considering simpler initial conditions, e.g. piecewise-constant initial conditions with finitely many jumps. For each $u_0 \in \mathcal{U}$ there is a sequence of initial $u_0^{(i)}$ that is a member of

$$(2.3) \quad \bar{\mathcal{U}} := \{v \in \mathcal{U} \cap P_0(\Omega_x) \mid v \text{ has finitely many jumps}\}$$

whose corresponding solution $u^{(i)}(\cdot, t)$ converge to $u(\cdot, t)$ in $L^1(\Omega_x)$ uniformly for all $t \in \Omega_t$. This fact is used for constructing approximations to the solution; see for example [18, 19]. As a result, we can focus on initial conditions $u_0 \in \bar{\mathcal{U}}$. In this case, it is known that the solution u only has discontinuities along finitely many rectifiable curves in Ω [76].

Unlike the familiar setting in which one *seeks* solutions to the initial value problem knowing only the initial condition u_0 , our focus here is to *reformulate* the entropy solution in a simplified form. Accordingly, we will freely make use of the knowledge of the solution u .

Assuming that the solution $u \in C(\Omega_t; L^1(\Omega_x))$ is known, we will first describe the characteristic curves. Let us define the function $G : \Omega_x \times \Omega_t \rightarrow \mathbb{R}$,

$$(2.4) \quad G(X, t) := \begin{cases} F'(u(X, t)) & \text{if } \llbracket u(X, t) \rrbracket = 0, \\ \frac{\llbracket F(u(X, t)) \rrbracket}{\llbracket u(X, t) \rrbracket} & \text{if } \llbracket u(X, t) \rrbracket \neq 0, \end{cases}$$

where $\llbracket v(x, t) \rrbracket := v(x_+, t) - v(x_-, t)$ denotes the difference between right and left limits of $v(\cdot, t)$ at x . The function G yields the velocity of the classical characteristic curves if the point $(X, t) \in \Omega$ lies in a smooth part of u , or yields the shock speed via the Rankine-Hugoniot jump conditions if it lies on a shock curve where u is discontinuous.

Characteristic curves of the initial value problem (2.1) are given by the solutions $X : \Omega_x \times \Omega_t \rightarrow \mathbb{R}$ to the family of ordinary differential equations

$$(2.5) \quad \frac{\partial X}{\partial t} = G(X, t), \quad X(x, 0) = x, \quad (x, t) \in \Omega_x \times \Omega_t.$$

This formulation for the characteristic curves is also called *generalized characteristics* [19]. It is straightforward to see that the problem (2.5) has a unique solution. This is due to the following: The RHS G is locally continuous, so the unique solution exists locally where it is continuous [33]; the solution is uniformly stable in neighborhoods of the points of discontinuity due to the entropy conditions, and at points of discontinuity the shock curve is also uniquely determined by the Rankine-Hugoniot jump conditions [76]. One also observes that the unique solution X is a continuous function of the initial value x , as G is of bounded variation.

Let us define the modified version of G by letting $G : \Omega_x \times \Omega_x \times \Omega_t \rightarrow \mathbb{R}$ be

$$(2.6) \quad G(X, x, t) := \begin{cases} F'(u_0(x)) & \text{if } \llbracket u(X, t) \rrbracket = 0, \\ \frac{\llbracket F(u(X, t)) \rrbracket}{\llbracket u(X, t) \rrbracket} & \text{if } \llbracket u(X, t) \rrbracket \neq 0. \end{cases}$$

We refer to both functions (2.5) and (2.6) as G and distinguish them by the number of the independent variables (i.e. number of input arguments).

Since our problem has no source terms (2.1), the solution is constant along the characteristic curves. So we may rewrite (2.5) as follows,

$$(2.7) \quad \frac{\partial X}{\partial t} = G(X, x, t), \quad X(x, 0) = x.$$

It is well-known that the characteristic curves may not fill all of Ω , so a similarity solution is sought to obtain the solution in all of the space-time domain Ω [50]. The set of points in the space-time domain Ω that cannot be connected to a point in $\Omega_x \times \{0\}$ by a characteristic curve is given by

$$(2.8) \quad \mathcal{R} := \{(x, t) \in \Omega \mid x \in \Omega_x \setminus X(\Omega_x, t)\}.$$

We will reformulate the similarity solutions as follows. Note that there exist two functions $\xi : \mathcal{R} \rightarrow \mathbb{R}$ and $\bar{\xi} : \mathcal{R} \rightarrow \Omega_x$ with the relation

$$(2.9) \quad \xi(x, t) = \frac{x - \bar{\xi}(x, t)}{t}, \quad (x, t) \in \Omega,$$

where $\bar{\xi}$ is a function that yields the origin of the rarefaction fan in Ω_x . This function is well-defined, since points in the rarefaction fan always have a unique origin [76].

We define a right inverse for nondecreasing real-valued function g defined on a real interval,

$$(2.10) \quad g^+(y) := \inf\{x \mid g(x) = y\}.$$

Throughout, the right inverse will always be applied to the spatial variable: That is, for functions of both variables $x \in \Omega_x$ and $t \in \Omega_t$, it will be applied solely to the spatial variable x .

The entropy solution u is then given in all of $\Omega_x \times \Omega_t$ by the formula

$$(2.11) \quad u(x, t) = \begin{cases} u_0(X^+(x, t)) & \text{if } (x, t) \in \Omega \setminus \mathcal{R}, \\ (F')^{-1}(\xi(x, t)) & \text{if } (x, t) \in \mathcal{R}. \end{cases}$$

2.2 Rarefied characteristics In this section, we modify the differential equation describing the characteristic curves (2.7), so that the form of the entropy solution (2.11) can be simplified. The modified form of the solution combines the two cases into just one. We shall achieve this by extending the initial condition u_0 and the characteristic curves X to an extended spatial domain that is larger than the original spatial domain Ω_x .

Observe that the set $\bar{\xi}(\mathcal{R})$ is a finite union of single points, since there are only finitely many jumps in the piecewise constant initial condition $u_0 \in \bar{\mathcal{U}}$ from which the rarefaction fans originate. Let $n_{\mathcal{R}} := |\bar{\xi}(\mathcal{R})|$ then we order and enumerate these by

$$(2.12) \quad \bar{\xi}(\mathcal{R}) = \{\xi_1 < \xi_2 < \dots < \xi_{n_{\mathcal{R}}}\}.$$

Correspondingly, we define a partition of $\mathcal{R} = \bigcup_{k=1}^{n_{\mathcal{R}}} \mathcal{R}_k$ by the following sets,

$$(2.13) \quad \mathcal{R}_k := \{(x, t) \in \mathcal{R} \mid \bar{\xi}(x, t) = \xi_k\}.$$

They are subsets of cones in Ω associated with a rarefaction fan emanating from a point $(\xi_k, 0) \in \Omega$.

Let us define a collection of $n_{\mathcal{R}}$ positive numbers $\varepsilon_k = u_0(\xi_{k+}) - u_0(\xi_{k-})$ so that $\sum_{k=1}^{n_{\mathcal{R}}} \varepsilon_k = |u_0|_{PV(\Omega_x)}$, the positive variation of u_0 [39] given by

$$(2.14) \quad |u_0|_{PV(\Omega_x)} = \sup_{x_0 < x_1 < \dots < x_N} \sum_i \max\{u_0(x_i) - u_0(x_{i-1}), 0\},$$

where the supremum is taken over any set of points $x_0 < x_1 < \dots < x_N$ lying in Ω_x and for any $N \in \mathbb{N}$. Then for each $k \in \mathbb{N}$, define the largest and smallest characteristic velocities in the rarefaction fans by

$$(2.15) \quad \nu_k^+ := \sup_{(x, t) \in \mathcal{R}_k} \frac{x - \xi_k}{t}, \quad \nu_k^- := \inf_{(x, t) \in \mathcal{R}_k} \frac{x - \xi_k}{t}.$$

Note that ν_k^{\pm} necessarily take on finite values [76].

Then we define an extended spatial domain $\hat{\Omega}_x$ as an interval given by

$$(2.16) \quad \hat{\Omega}_x := \left(0, 1 + \sum_{k=1}^{n_{\mathcal{R}}} \varepsilon_k\right) = \left(0, 1 + |u_0|_{PV(\Omega_x)}\right).$$

We embed Ω_x into $\hat{\Omega}_x$ via the map $\iota : \Omega_x \rightarrow \hat{\Omega}_x$

$$(2.17) \quad \iota(x) := x + \sum_{\{k: \xi_k < x\}} \varepsilon_k,$$

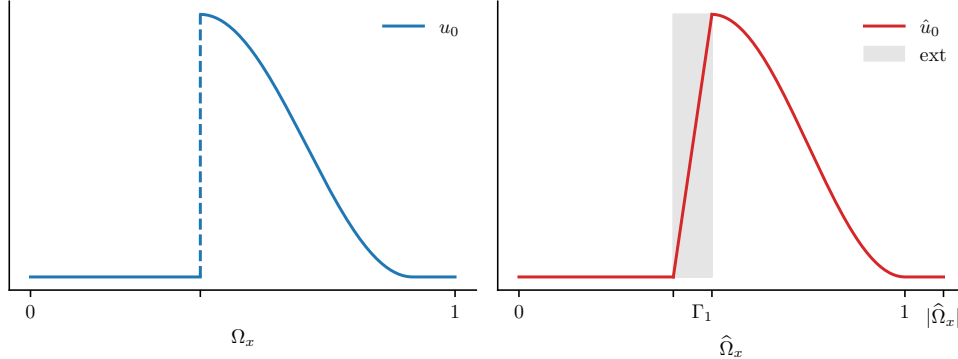


Fig. 2.1: An example of an extended initial condition \hat{u}_0 of u_0 in the case of Burgers' flux. The newly assigned values of \hat{u}_0 in the interval Γ_1 are given by (2.20). The values are linear due to the choice of the Burgers' flux.

and assign intervals Γ_k of length ε_k starting at $\iota(\xi_k)$,

$$(2.18) \quad \Gamma_k := \iota(\xi_k) + (0, \varepsilon_k], \quad \Gamma_x := \bigcup_{k=1}^{n_{\mathcal{R}}} \Gamma_k.$$

That is, the extended domain $\hat{\Omega}_x$ is a longer interval where Γ_k have been inserted into points in $\{\xi_k\} \subset \Omega_x$. That is, $\hat{\Omega}_x = \iota(\Omega_x) \cup \Gamma_x$ and $\hat{\Omega}_x$ is larger than Ω_x by some length

$$(2.19) \quad |\Gamma_x| = \sum_{k=1}^{n_{\mathcal{R}}} |\Gamma_k| = \sum_{k=1}^{n_{\mathcal{R}}} \varepsilon_k = |u_0|_{PV(\Omega_x)},$$

where $|\cdot|$ denotes the measure of a set. Next we extend the initial condition u_0 to $\hat{\Omega}_x$ by letting $\hat{u}_0 : \hat{\Omega}_x \rightarrow \mathbb{R}$ be given as

$$(2.20) \quad \hat{u}_0 \circ \iota := u_0, \quad \hat{u}_0 \Big|_{\Gamma_k} := (F')^{-1} \left(\nu_k^- + \frac{\nu_k^+ - \nu_k^-}{\varepsilon_k} (x - \iota(\xi_k)) \right).$$

Then \hat{u}_0 has no positive jumps (entropy violating shocks [76]) and has the same total variation as u_0 ,

$$(2.21) \quad |\hat{u}_0|_{TV(\Omega_x)} = |u_0|_{TV(\hat{\Omega}_x)}.$$

Intuitively speaking, one obtains \hat{u}_0 from u_0 by replacing positive jumps with continuous slopes, prescribed the similarity solution. See Fig. 2.1 for an illustration comparing u_0 and \hat{u}_0 .

We define *rarefied characteristic curves* $\hat{X} : \hat{\Omega}_x \times \Omega_t \rightarrow \Omega_x$ as the solution to the differential equation

$$(2.22) \quad \frac{\partial \hat{X}}{\partial t} = \hat{G}(\hat{X}, x, t), \quad \hat{X}(x, 0) = \hat{I}(x),$$

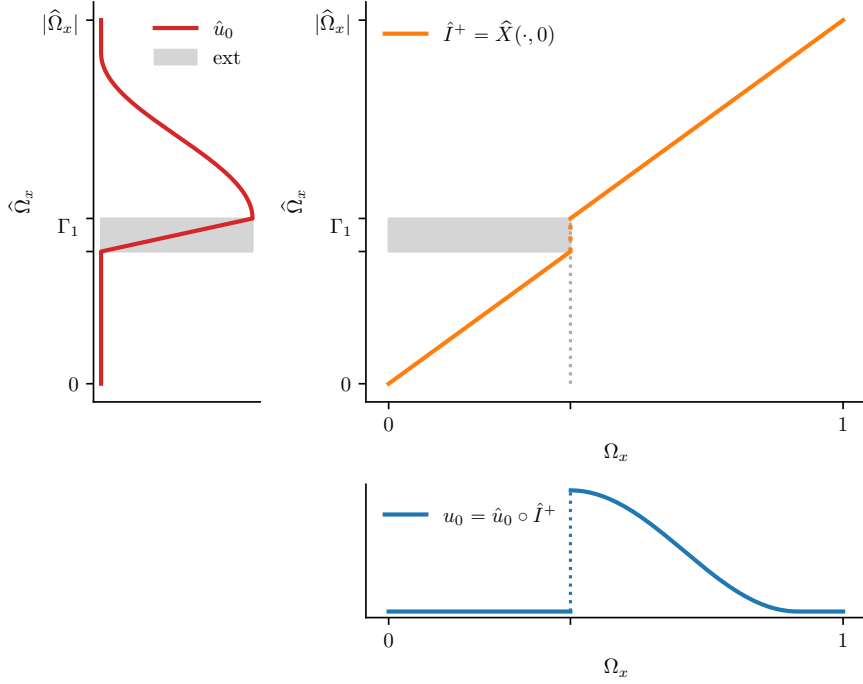


Fig. 2.2: An example of the extension u_0 to \hat{u}_0 as in (2.20) for the Burgers flux $F(u) = u^2/2$. The function \hat{I}^+ has a jump discontinuity of magnitude $|\Gamma_1|$ as depicted in the upper right plot. Due to this jump, the values of \hat{u}_0 inside interval Γ_1 highlighted in the upper left plot are effectively omitted in the composed function $\hat{u}_0 \circ \hat{I}^+$. This effect is shown in the lower right plot.

where $\hat{I} : \hat{\Omega}_x \rightarrow \Omega_x$ is a continuous piecewise linear function satisfying $\hat{I}^+ = \iota$ given by

$$(2.23) \quad \hat{I}(0) = 0, \quad \hat{I}' = \mathbf{1}_{\hat{\Omega}_x \setminus \Gamma_x},$$

and $\hat{G} : \Omega_x \times \hat{\Omega}_x \times \Omega_t \rightarrow \mathbb{R}$ is an extension of G (2.6),

$$(2.24) \quad \hat{G}(\hat{X}, x, t) := \begin{cases} F'(\hat{u}_0(x)) & \text{if } \llbracket u(\hat{X}, t) \rrbracket = 0, \\ \frac{\llbracket F(u(\hat{X}, t)) \rrbracket}{\llbracket u(\hat{X}, t) \rrbracket} & \text{if } \llbracket u(\hat{X}, t) \rrbracket \neq 0. \end{cases}$$

The nonlinear RHS term (2.24) of the ODE (2.22) can be written as a function of bounded variation that depends only on \hat{X} and t . This implies that $\hat{X}(\cdot, t)$ is non-decreasing for all $t \in \Omega_t$, regardless of whether u_0 has jumps (see, e.g. Ch. 5 of [33]); positive jumps of u_0 are replaced by continuous pieces in $\hat{\Omega}_x$, negative jumps are replaced by piecewise constants.

See Fig. 2.2 for an illustration showing \hat{I} and its role in relating u_0 with \hat{u}_0 (2.22). A diagram depicting the evolution of \hat{X} is shown in Fig. 2.3.

LEMMA 2.1. *The entropy solution u to (2.1) is given by*

$$(2.25) \quad u(x, t) = \hat{u}_0 \circ \hat{X}^+(x, t).$$

Recall that $(\cdot)^+$ denotes the left-inverse (2.10).

Proof. See Appendix B.1. \square

We make a couple of remarks here. Note that new shocks cannot form at $\hat{X}(x_0, t)$ for $x_0 \in \Gamma_x$ since the solution to (2.22) is strictly increasing with respect to x at x_0 . So the solution given by (2.25) at the points $(\hat{X}(x_0, t), t)$, for times before $\hat{X}(x_0, \cdot)$ enters a shock, agrees with the expression for the rarefaction fan. These observations imply that \hat{X} is continuous.

Let us define the *rarefied characteristic curves with multivalued inverse*,

$$(2.26) \quad \hat{X}_0(x, t) := \hat{I}(x) + t(F' \circ \hat{u}_0)(x)$$

which is in $\text{span}\{\hat{I}, F' \circ \hat{u}_0\}$. This map represents the classical characteristic curves and the rarefaction waves but represents the overturned multivalued solution, instead of using shocks [50].

2.3 Shock time function Here we will define the shock time function, which we will be a crucial component in our constructions in the later sections.

Let us define the parametrized set we call the *shock set* Υ_t for $t \in \Omega_t$ to contain all $x \in \hat{\Omega}_x$ such that the preimage of the singleton $\{x\}$ given by $\hat{X}^{-1}(\hat{X}(\{x\}, t), t)$ is non-unique. That is,

$$(2.27) \quad \Upsilon_t := \left\{ x \in \hat{\Omega}_x \mid \exists y \in \Omega_x \text{ such that } y \neq x, \hat{X}(x, t) = \hat{X}(y, t) \right\}.$$

Then $(\Upsilon_t)_{t \in \Omega_t}$ is non-decreasing with respect to $t \in \Omega_t$, i.e. for $0 \leq t_1 \leq t_2 \leq T$ we have $\Upsilon_{t_1} \subset \Upsilon_{t_2}$ due to the entropy conditions which ensure the characteristics merge into the shock. Since \hat{X} is a non-decreasing continuous function of x for all t as noted above, Υ_t is closed for all $t \in \Omega_t$. In plain terms, the set Υ_t are points in the extended spatial domain $x_0 \in \hat{\Omega}_x$ such that, the rarefied characteristic curve leaving from the point $\hat{X}(x_0, \cdot)$ has merged into a shock at a time before t .

We define a function $\lambda : \Upsilon_T \rightarrow \Omega_t$ we call the *shock time function*, given in terms of its level sets. Specifically, let λ be given by

$$(2.28) \quad \left\{ x \in \hat{\Omega}_x \mid \lambda(x) \leq t \right\} = \Upsilon_t.$$

Note that Υ_t is closed for all $t \in \Omega_t$; $\hat{X}(\cdot, t)$ is non-decreasing and continuous, implying that Υ_t is a union of disjoint closed intervals. It follows that λ is continuous: a closed set D lying in Ω_t is compact, and moreover Υ_t is increasing in t , hence we have $\lambda^{-1}(D) = \Upsilon_{\max D}$, which is closed.

In intuitive terms, the value $\lambda(x)$ is the time the characteristic curve starting from $x \in \Upsilon_T \subset \hat{\Omega}_x$ merges into a shock.

It is left to the reader to show that \hat{X} is related to \hat{X}_0 by the relation,

$$(2.29) \quad \hat{X}(x, t) = \sup_{\substack{y < x \\ y \in \hat{\Omega}_x \setminus \Upsilon_t}} \hat{X}_0(y, t),$$

yielding an alternative formulation of \hat{X} that reveals it is simply \hat{X}_0 with certain portions replaced by a constant regions.

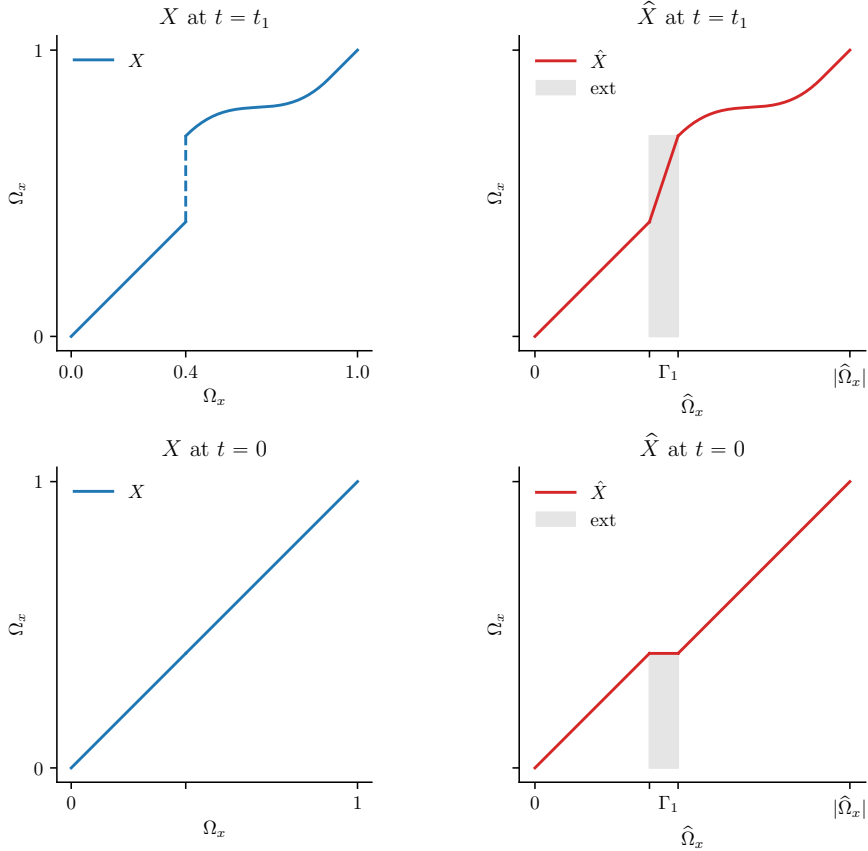


Fig. 2.3: An illustration comparing the characteristic curves X (left) with the evolution of rarefied characteristics \hat{X} at some later time $t_1 > 0$ (right).

2.4 Compositional form In the previous section, we have simplified the expression of the entropy solution from (2.11) to (2.29), by incorporating the evolution of the rarefaction waves into the characteristic curves in (2.22). Next, we simplify how the shock is represented in \hat{X} .

In the case of classical solutions, the characteristic curves (2.5) are represented by a linear superposition,

$$(2.30) \quad X(x, t) = x + t(F' \circ u_0)(x) \in \text{span}\{\text{Id}, F' \circ u_0\}.$$

We wish to rewrite $\hat{X}(x, t)$ in a form with similar linear superpositions, modulo compositions and left-inverses. Note that one can show the family of functions $\{\hat{X}(\cdot, t) \mid t \in \Omega_t\}$ can have a slowly decaying Kolmogorov width, except in special cases with simple initial data u_0 . Consider the stationary shock example shown in Fig. 2.4. The shock is represented by the constant region Υ_t in \hat{X} , which is expanding over time. The jump in the derivative in \hat{X} travels to the left and the right, which cannot be efficiently represented by the superposition of a few basis functions.

Our key idea is to cut out the portion of the domain where $\hat{X}_0(\cdot, t)$ represents the

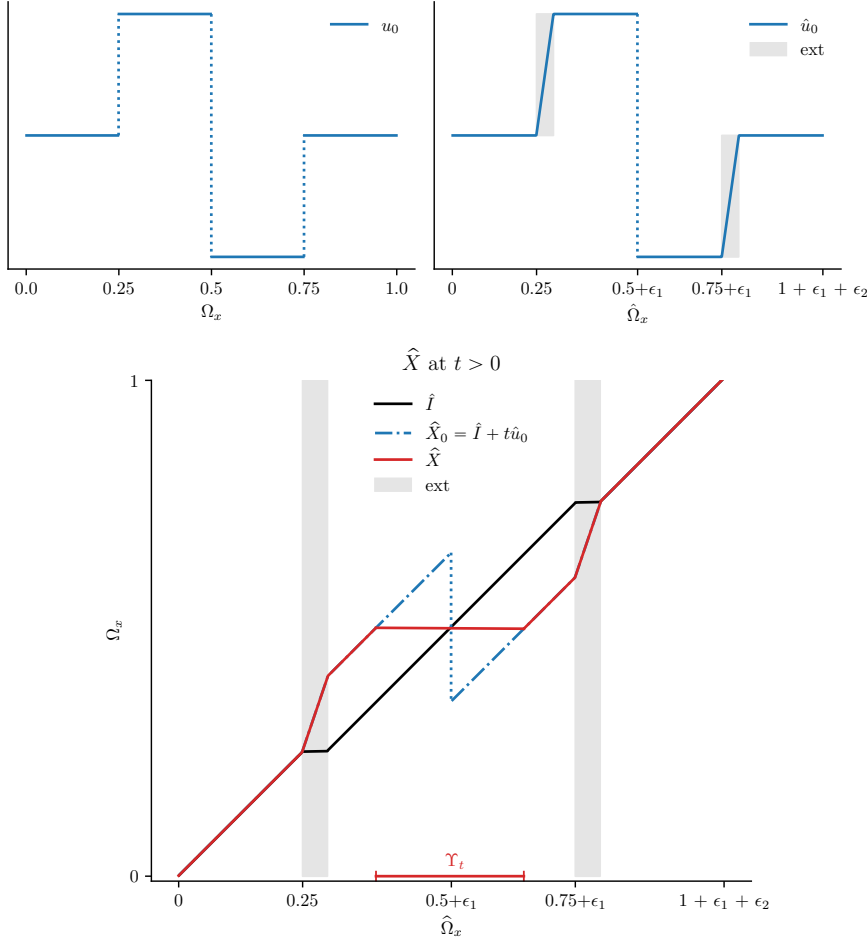


Fig. 2.4: A stationary shock example for the Burgers' equation. Due to the jump discontinuity in the initial condition \hat{u}_0 located at $x = 0.5$, the shock forms immediately at initial time. This shock is represented as the constant part of the function \hat{X} in Υ_t , and the left-inverse of the rarefied characteristic \hat{X}^+ has a jump discontinuity there. As time evolves, the characteristics merge into the shock, so Υ_t where \hat{X} is constant correspondingly expands over time. Consequently, the kinks in \hat{X} at the left and right endpoints of Υ_t travel to the left and to the right, respectively. (For a plot of the evolution of the rarefied characteristics, see Fig. 5.1 below.)

shock, by adding the characteristic function of Υ_t to it. Let us denote the threshold function by $\rho := \mathbf{1}_{\mathbb{R}_+}$. We call the modified curves the *relief characteristic curves*, given by

$$(2.31) \quad \check{X} = \hat{I} + t(F' \circ \hat{u}_0) + C_x \rho \circ (t - \lambda),$$

for some sufficiently large constant $C_x \geq |\Omega_x|$. Then, the entropy solution is written

as

$$(2.32) \quad u(x, t) = \hat{u}_0 \circ \check{X}^+(x, t).$$

Once the left-inverse is applied to \check{X} , the resulting map $\check{X}^+ : \Omega_x \rightarrow \hat{\Omega}_x$ is constant at points in Υ_t , because the term $\rho(t - \lambda(x))$ introduces the constant region and removes the portion of \check{X} which lies in Υ_t by adding a sufficiently large constant to \hat{X}_0 whenever it is evaluated at a point in Υ_t . See Fig. 2.5 for an illustration.

Written in a generic form, the solution is

$$(2.33) \quad u(\cdot, t) = \psi_1 \circ (\phi_1 + t\phi_2 + \phi_3 \circ (t\varphi_1 - \varphi_2))^+$$

where the individual functions are defined as

$$(2.34) \quad \psi_1 = \hat{u}_0, \quad \phi_1 = \hat{I}, \quad \phi_2 = F' \circ \hat{u}_0, \quad \phi_3 = C_x \rho, \quad \varphi_1 = 1, \quad \varphi_2 = \lambda.$$

We will call this the *compositional form of the entropy solution*.

In this representation, the time-dependence is in the coefficients of linear combinations within each composition, and the dependence of the coefficients with respect to t is linear, in a similar manner as the classical case. To elaborate, the first linear combination in (2.33) is $t\varphi_1 - \varphi_2$ with two coefficient values t and -1 . Only the first coefficient depends on t and the dependence is linear.

In the compositional form, the left-inverse $(\cdot)^+$ persists, leaving it an implicit form rather than an explicit one. When we consider the discretization of this form of the entropy solution, we will make use of a trick we call the *inverse-bias trick* that will allow us to avoid any direct evaluation of the left-inverse (Sec. 4.1).

We refer the reader to Appendix A for a glossary of various entropy solution formulations introduced in this section.

3 Low Rank Neural Representation We introduce a family of feedforward neural networks that satisfy a low rank condition. The condition is inspired by the fact that the entropy solution, represented using the relief characteristic curves (2.33), is made up of compositions of low rank representations. To make this point clear, we draw up a diagram of each step of the evaluation of (2.33) along with the associated linear spaces, as follows.

$$(3.1) \quad \begin{array}{ccc} x & & \\ \downarrow & \searrow & \\ x & t\varphi_1 - \varphi_2 & \text{span}\{\text{Id}, \varphi_1, \varphi_2\} \\ \downarrow & \downarrow & \\ \phi_1 + t\phi_2 + \phi_3 \circ (t\varphi_1 - \varphi_2) & & \text{span}\{\phi_1, \phi_2, \phi_3\} \\ \downarrow & & \\ \psi_1 \circ (\phi_1 + t\phi_2 + \phi_3 \circ (t\varphi_1 - \varphi_2))^+ & & \text{span}\{\psi_1\} \end{array}$$

For example, the operations in the second step can be written as

$$(3.2) \quad \begin{bmatrix} | & | & | \\ \phi_1(z) & \phi_2(z) & \phi_3(z) \\ | & | & | \end{bmatrix} \begin{bmatrix} 1 \\ t \\ 1 \end{bmatrix} \in \text{span}\{\phi_1, \phi_2, \phi_3\}$$

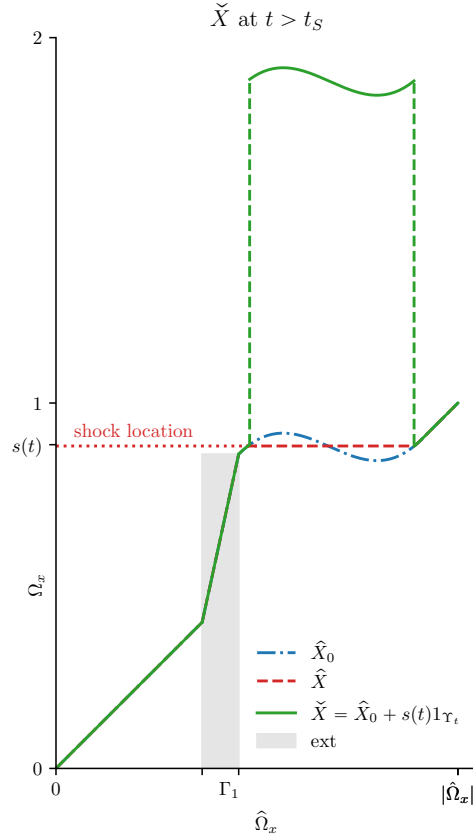


Fig. 2.5: A diagram depicting the relief characteristics \check{X} after shock formation time t_S is shown, along with the rarefied characteristics with multivalued inverse \hat{X}_0 . The relief characteristics use a different representation of the shock compared to the rarefied characteristics \hat{X} , one that uses the addition of a box function 1_{Γ_t} . One observes that left-inverse \check{X}^+ has a jump at $s(t)$, and this jump is identical to the corresponding one for \hat{X}^+ .

where $z = (x, t\varphi_1(x) - \varphi_2(x))^T$ is the output from the previous step. This expression is superposition of a few vectors, if one views the function values $\phi_i(z)$ as column vectors of infinite length. In addition, note that the individual the coefficients $[1, t, 1]^T$ has either a linear dependence on t or is constant.

This structure of repeated compositions closely resembles the repeated compositions in a neural network. The component that requires a close scrutiny is the left-inverse $(\cdot)^+$ and its treatment will be a key discussion in the coming sections (Sec. 4.1 and Sec. 5.1). For the moment, let us focus on establishing an analogy with feedforward neural networks. We begin by introducing notations and definitions of a neural network. Our notations are similar to those in common use (see, e.g. [22, 3], for similar definitions). Throughout, the superscript ℓ will index the layer number.

DEFINITION 3.1 (Feedforward neural network architecture). *Given the dimension*

sions $(M_0, M_1, \dots, M_L) \in \mathbb{N}^L$ let

$$(3.3) \quad \mathbb{W}^\ell := \{W : \mathbb{R}^{M_{\ell-1}} \rightarrow \mathbb{R}^{M_\ell} \mid W \text{ linear}\}, \quad \mathbb{B}^\ell := \mathbb{R}^{M_\ell},$$

and define the Cartesian products

$$(3.4) \quad \mathbb{W} := \bigtimes_{\ell=1}^L \mathbb{W}^\ell, \quad \mathbb{B} := \bigtimes_{\ell=1}^L \mathbb{B}^\ell.$$

We call the pair (\mathbb{W}, \mathbb{B}) a feedforward neural network architecture or simply architecture. We refer to $M = \max_\ell M_\ell$ as the width and L as the depth of the architecture.

DEFINITION 3.2 (Feedforward Neural Networks). Given an architecture (\mathbb{W}, \mathbb{B}) , a feedforward neural network (NN) with weights $W = (W^1, \dots, W^L) \in \mathbb{W}$ and biases $B = (B^1, \dots, B^L) \in \mathbb{B}$ is defined as the function $h : \mathbb{R} \rightarrow \mathbb{R}$ with

$$(3.5) \quad h(x; W, B) := A^L \circ \sigma \odot A^{L-1} \circ \dots \circ \sigma \odot A^1(x)$$

in which \odot is the entrywise composition, σ is the rectified linear unit (ReLU) $\sigma(x) = \max\{0, x\}$, and the affine maps A_ℓ are given by

$$(3.6) \quad A^\ell(z) = W^\ell z + B^\ell, \quad W^\ell \in \mathbb{W}^\ell, \quad B^\ell \in \mathbb{B}^\ell.$$

We will use the shorthand $h(W, B) := h(\cdot; W, B)$.

In what follows, we make the observation that the superpositions in between the compositions in (3.1) is analogous to the affine mappings that appear in the neural network (3.6). With this viewpoint, we show it is natural to consider a neural network with the affine mappings with low rank weights and biases, in correspondence to the low rank representation in (3.1). Let us consider the composition of two functions which are individually in the span of $\{\phi_i\}_{i=1}^r$ and $\{\varphi_i\}_{i=1}^r$, with the coefficients $\{\gamma_i^3\}_{i=1}^r$ and $\{\gamma_i^2\}_{i=1}^r$, resp.,

$$(3.7) \quad \left(\sum_{i=1}^r \gamma_i^3 \phi_i \right) \circ \left(\sum_{i=1}^r \gamma_i^2 \varphi_i \right) (x),$$

which is a general form of the first composition in (3.1). For the simple scenario $r = 1$ and both $\phi_1, \varphi_1 : \mathbb{R} \rightarrow \mathbb{R}$ are scalar valued 1d functions representable by 2-layer NNs, their composition has the structure shown in black and grey below,

$$(3.8) \quad \begin{aligned} & (\gamma_1^3 \phi_1) \circ (\gamma_1^2 \varphi_1)(x) \\ &= \gamma_1^3 \left[\dots \dots \right] \sigma \odot \underbrace{\left(\gamma_1^2 \begin{bmatrix} \vdots \\ \vdots \end{bmatrix} \left[\dots \dots \right] \sigma \odot \left(\begin{bmatrix} \vdots \\ \vdots \end{bmatrix} [x] + \begin{bmatrix} \vdots \\ \vdots \end{bmatrix} \right) + \begin{bmatrix} \vdots \\ \vdots \end{bmatrix} [\cdot] \right)}_{W^2} + [\cdot]. \end{aligned}$$

In particular, the weight matrix of the second layer is rank one:

$$(3.9) \quad W^2 = \gamma_1^2 U_1^2, \quad U_1^2 \text{ is rank-1.}$$

Likewise, multiple scalar functions $\{\phi_i\}_{i=1}^r$ and $\{\varphi_i\}_{i=1}^r$ lead one to feedforward neural networks (3.5) whose weights and biases (3.6) are formed as linear combinations of

rank-1 matrices in each layer. Assuming $r \ll M$, we have arrived at a low-rank form of the weight matrix.

This derivation illustrates that, in looking for a low-dimensional description of entropy solutions, it is natural to turn our attention to neural networks whose weights W and biases in B are represented as linear combinations of a few rank-1 linear transformations. For example, we require that

$$(3.10) \quad W^\ell = \sum_{i=1}^r \gamma_i^\ell U_i^\ell, \quad B^\ell = \sum_{i=1}^r \theta_i^\ell V_i^\ell, \quad \begin{cases} \gamma_i^\ell, \theta_i^\ell \in \mathbb{R}, \\ U_i^\ell \in \mathbb{W}^\ell, V_i^\ell \in \mathbb{B}^\ell \text{ are rank-1,} \\ \ell = 1, \dots, L. \end{cases}$$

The coefficients $\{\gamma_i^\ell, \theta_i^\ell\}$ correspond to the coefficients $\{1, t\}$ used in the linear combinations at each compositional step in (3.1). One notes that the latter coefficients depend on the parameter t (the time variable), and the role of this parameter is different from either the input x or the fixed weights and biases $\{U_i^\ell, V_i^\ell\}$ prescribing the linear spaces the weights and biases belong to. It is therefore natural to view the coefficients $\{\gamma_i^\ell, \theta_i^\ell\}$ as distinct external parameters; a specific coefficient set $\{\gamma_i^\ell, \theta_i^\ell\}$ correspond to a specific neural network belonging to the family of neural networks whose weights and biases satisfy (3.10). The dependence on t in (3.1) would correspond to the dependence of the coefficients $\{\gamma_i^\ell, \theta_i^\ell\}$ on t . On the other hand, the fixed weights and biases correspond to the functions in the low rank representation that do not depend on t , e.g. the functions $\{\varphi_i, \phi_j, \psi_k\}$ in (3.2).

Motivated by these observations, we define a family of neural networks in which (1) all of its members have weights and biases that lie in a fixed low-dimensional linear space, and (2) the particular coefficients that determine a specific neural network within that family is treated as a special external parameter.

Let us set a notation for linear combinations. Given a linear space \mathbb{V} , let $\Phi_r = (\phi_i)_{i=1}^r \subset \mathbb{V}$ and $A \subset \mathbb{R}^r$, then let

$$(3.11) \quad A \cdot \Phi_r := \left\{ \sum_{i=1}^r \alpha_i \phi_i \mid \alpha \in A \right\}.$$

We denote by \otimes the Kronecker product, and introduce the Hadamard-Kronecker products $\otimes_d : \mathbb{R}^{m_1} \times \mathbb{R}^{m_2} \rightarrow \mathbb{R}^{m_1 m_2 \times m_2}$ and $d\otimes : \mathbb{R}^{m_1} \times \mathbb{R}^{m_2} \rightarrow \mathbb{R}^{m_1 \times m_1 m_2}$ between two vectors as follows,

$$(3.12) \quad u^L \otimes_d u^R := u^L \otimes \text{diag}(u^R), \quad u^L \cdot_d u^R := \text{diag}(u^L) \otimes u^R.$$

We now define the family of neural networks that is central to this paper.

DEFINITION 3.3 (Low Rank Neural Representation (LRNR)). *Let us be given*

- (i) *an architecture (\mathbb{W}, \mathbb{B}) of depth L and width M ,*
- (ii) *members of \mathbb{W}_ℓ and \mathbb{B}_ℓ for each $\ell = 1, \dots, L$,*

$$(3.13) \quad \mathbb{U}_r^\ell := (U_i^\ell)_{i=1}^r \subset \mathbb{W}^\ell, \quad \mathbb{V}_r^\ell := (V_i^\ell)_{i=1}^r \subset \mathbb{B}^\ell,$$

in which U_i^ℓ and V_i^ℓ are the products of two vectors

$$(3.14) \quad \begin{cases} U_i^\ell = u_i^{\ell, L} \bullet u_i^{\ell, R}, \\ V_i^\ell = v_i^{\ell, L} \bullet' v_i^{\ell, R}, \end{cases} \quad \text{where} \quad \bullet, \bullet' \in \{\otimes, d\otimes, \otimes_d\},$$

(iii) coefficient sets $C^\ell, D^\ell \subset \mathbb{R}^r$ collected in

$$(3.15) \quad C := \bigtimes_{\ell=1}^L C^\ell, \quad D := \bigtimes_{\ell=1}^L D^\ell.$$

Let us denote

$$(3.16) \quad \mathbb{W}_r := \bigtimes_{\ell=1}^L (C^\ell \cdot \mathbb{U}_r^\ell) \subset \mathbb{W}, \quad \mathbb{B}_r := \bigtimes_{\ell=1}^L (D^\ell \cdot \mathbb{V}_r^\ell) \subset \mathbb{B}.$$

Then a LRNR is defined as the parametrized family of feedforward neural networks

$$(3.17) \quad H_r := \{h(W, B) \mid W \in \mathbb{W}_r, B \in \mathbb{B}_r\}.$$

We denote by $h(\gamma, \theta)$ the NN $h \in H_r$ that is associated with $(\gamma, \theta) \in C \times D$. For the LRNR H_r we shall refer to r as its rank. Denote by K the degrees of freedom (d.o.f), that is, the number of trainable or stored parameters, M its width, and L its depth. One necessarily has $K \lesssim rLM$.

The d.o.f refer to the set of parameters appearing in the weights or biases that is unconstrained. In deep learning models, weight parameters are often constrained in various ways, e.g. to be equal to each other, and these constrained parameters are commonly referred to as *shared* weights [30]. As an example, a one dimensional convolution layer with a single channel and a kernel of width three has d.o.f $K = 3$ but the width of that layer M may be different.

We remark that in the LR-PINNs [13] the coefficient $\theta_{i,\ell}$ for the biases were treated as fixed, and the coefficients $\gamma_{i,\ell}$ were functions of the parameters of the PDE.

In summary, a LRNR is a family of feedforward networks that have weights and bias at each individual layer that belong to a fixed linear subspace of dimension at most r . The aim of the following sections is to establish the connection between LRNR (Def. 3.3) and the entropy solution (3.1). Throughout this work, our focus is on scalar problems in a single spatial dimension, so the input and output dimensions are one, that is, $M_0 = M_L = 1$.

We refer the reader to Appendix A for a glossary of various notations and specifications regarding LRNRs introduced in this section.

4 LRNR approximation of classical solutions In this section, we will discuss how a LRNR can be used to approximate classical solutions to (2.1). In this case, the solution is given by the method of characteristics (2.30), and is known to have an efficient approximation using transported subspaces [71]. For the classical case, it is mandatory to suspend the assumption that the initial condition is piecewise constant with finitely many jumps (that is, $u_0 \in \bar{\mathcal{U}}$). Then, for a smooth initial condition $u_0 \in \mathcal{U}$ (2.2) the classical solution is

$$(4.1) \quad u(x, t) = u_0 \circ X^{-1}(x, t),$$

with classical characteristics X that solve the ODE (simpler version of (2.4)),

$$(4.2) \quad \frac{\partial X}{\partial t} = F'(u(X, t)), \quad X(x, 0) = x, \quad (x, t) \in \Omega_x \times \Omega_t.$$

Due to the absence of rarefaction and shock waves in the classical case, the solutions simplifies in two major ways: (1) The inverse $(\cdot)^{-1}$ is used in the solution (4.1) rather than the left-inverse $(\cdot)^+$ used in (2.25, 2.32), and (2) the initial condition u_0 and the characteristic curves X are directly used instead of their extensions (i.e. \hat{u}_0 , \hat{X} or \check{X}).

We focus on the fact that the classical solution (4.1) resembles the compositions of superpositions (3.7) we have encountered when deriving LRNRs in the previous section. We may write the classical solution in a similar form,

$$(4.3) \quad u(x, t) = \left(\sum_{i=1}^r \gamma_i^2(t) \phi_i \right) \circ \left(\sum_{i=1}^r \gamma_i^1(t) \varphi_i \right)^{-1} (x)$$

with $r = 3$ and
$$\begin{cases} \gamma_1^1 = 1, & \gamma_2^1 = t, & \gamma_3^1 = 0, \\ \varphi_1 = \text{Id} & \varphi_2 = F' \circ u_0, \\ \gamma_1^2 = 1, & \gamma_2^2 = 0, & \gamma_3^2 = 0, \\ \phi_1 = u_0. \end{cases}$$

An important difference with (3.7) is the presence of the inverse $(\cdot)^{-1}$. This must be carefully handled to approximate this compositional form of the classical solution using LRNRs. This issue arose in the compositional reduced models and other neural network approximations [78, 47, 71]. Our discussion here centers specifically on transported subspaces [71] which are most directly related to LRNRs.

We will recall the transported subspaces, and discuss how the inverse that appears in the composition can be avoided straightforwardly using a trick we call the *inverse-bias trick*. Starting with a given transported subspace in its original form, we will first show that one can rewrite it in a certain discrete form using this trick. Next, we will show that a transported subspace in this discrete form is equivalent to a 2-layer LRNR of comparable complexity. Finally, we will approximate the classical solution to the scalar conservation law using a 2-layer LRNR. The techniques developed in this section for approximating the classical solutions will be used throughout the subsequent Sec. 5 that addresses the entropy solution. We refer the reader to Appendix A for a summary of notions including the transported subspaces, the inverse-bias trick, and the LRNR approximation of the classical solution introduced in this section.

4.1 The transported subspaces and the inverse-bias trick We will review the definition of transported subspaces and introduce an approximation technique which allows one to avoid calculating the left-inverses that typically appear in method of characteristics, e.g. in (2.30, 2.33). Then we will derive a useful estimate for transport subspaces when this technique is applied.

Throughout this section and the next, we will use the notation Ω_x and $\hat{\Omega}_x$ to denote arbitrary open intervals in \mathbb{R} , however in the subsequent sections they will play roles analogous to the spatial domain in (2.1) and the extended spatial domain (2.16) above.

DEFINITION 4.1 (Admissible coefficients). *Given a domain $\Omega_x \subset \mathbb{R}$ and a set of r functions $\Phi_r = (\phi_i)_{i=1}^r \subset P_1(\mathbb{R}) \cap C(\mathbb{R})$ we say a coefficient set $A \subset \mathbb{R}^r$ is admissible for Φ_r on Ω_x if*

- (i) *there exist constants $c_A, C_A > 0$ such that $c_A \leq g' \leq C_A$ for all $g \in A \cdot \Phi_r$,*
- (ii) *$g(\mathbb{R}) \supset \Omega_x$ for all $g \in A \cdot \Phi_r$.*

We will also write $\hat{\Omega}_x := \bigcup_{g \in A \cdot \Phi_r} g^{-1}(\Omega_x)$.

DEFINITION 4.2 (Transported subspace). *Suppose we are given a domain $\Omega_x \subset \mathbb{R}$, linearly independent functions*

$$(4.4) \quad \begin{aligned} \Phi_r &= (\phi_i)_{i=1}^r \subset P_1(\mathbb{R}) \cap C(\mathbb{R}), \\ \Psi_r &= (\psi_i)_{i=1}^r \subset P_0(\mathbb{R}) \cap BV(\mathbb{R}), \end{aligned}$$

and two coefficient sets, $A \subset \mathbb{R}^r$ admissible for Φ_r on Ω_x and $B \subset \mathbb{R}^r$ bounded.

The transported subspace is the family H_r given by

$$(4.5) \quad \begin{aligned} \bar{H}_r &:= (B \cdot \Psi_r) \circ (A \cdot \Phi_r)^{-1} \\ &= \{\bar{h} \in P_0(\Omega_x) \cap BV(\Omega_x) \mid \bar{h} = f \circ g^{-1}, f \in B \cdot \Psi_r, g \in A \cdot \Phi_r\}. \end{aligned}$$

We denote by $\bar{h}(\alpha, \beta)$ the member $\bar{h} \in \bar{H}_r$ where $(\alpha, \beta) \in A \times B$.

The functions in Φ_r and Ψ_r can be viewed as reduced basis functions or snapshots.

Next, we introduce the inverse-bias trick. Observe the important advantages in choosing Ψ_r to be a set of piecewise constant functions. Expressing a member $f \in B \cdot \Psi_r$ as the sum

$$(4.6) \quad f(x) = c_0 + \sum_k c_k \rho(x - x_k),$$

the transported function $h = f \circ g^{-1}$ for $g \in A \cdot \Phi_r$ can be rewritten

$$(4.7) \quad f \circ g^{-1}(x) = c_0 + \sum_k c_k \rho(g^{-1}(x) - x_k) = c_0 + \sum_k c_k \rho(x - g(x_k)).$$

In this form one readily observes that the dependence of h on the function g is only at the discrete set of points $\{x_k\}$, and that the inverse g^{-1} is replaced by the forward map g . This follows from the simple fact that the monotonicity of g implies

$$(4.8) \quad \begin{aligned} \rho(g^{-1}(x) - x_k) &= \begin{cases} 1 & \text{if } g^{-1}(x) \geq x_k, \\ 0 & \text{if } g^{-1}(x) < x_k, \end{cases} \\ &= \begin{cases} 1 & \text{if } x \geq g(x_k), \\ 0 & \text{if } x < g(x_k), \end{cases} \\ &= \rho(x - g(x_k)). \end{aligned}$$

We refer to this technique of removing the inverse applied to g by instead applying the forward map g on the bias terms, the *inverse-bias trick*.

Careful consideration in Lem. 4.3 below shows that the inverse bias trick applies to non-decreasing functions that have a left-inverse but not necessarily an inverse. While in this paper analytical expression for g originate from hyperbolic conservation laws and are thus left-invertible, we do not require invertibility of their numerical approximations g_ε . Indeed, since the right hand side of the inverse bias trick is independent of the inverse, we have $\rho(g^{-1}(x) - x_k) = \rho(x - g(x_k)) \approx \rho(x - g_\varepsilon(x))$ for which we can easily control the error without assuming invertibility of g_ε , as e.g. in Lem. 4.3. In principle, one can further apply the right hand side to arbitrary non-invertible functions g such as multi-valued characteristics at shocks, but this would invalidate the left hand side and with it the original meaning of the identity. For such cases, we require additional techniques, as we discuss in Sec. 5. Note that this

issue of invertibility has been a source of difficulties discussed in related approaches [38, 9, 78].

In the following lemma the approximating function is continuous and piecewise linear; therein the jump function ρ is replaced by a continuous piecewise linear approximation ρ_ε defined as

$$(4.9) \quad \rho_\varepsilon(x) := \frac{1}{\varepsilon} \left[\sigma(x + \frac{\varepsilon}{2}) - \sigma(x - \frac{\varepsilon}{2}) \right].$$

For a finite set $\mathcal{X} \subset \hat{\Omega}_x$ and $g : \hat{\Omega}_x \rightarrow \mathbb{R}$, we will make use of the discrete norm $\|g\|_{L^\infty(\mathcal{X})} := \max_{x_i \in \mathcal{X}} |g(x_i)|$.

LEMMA 4.3. *Let $f : \mathbb{R} \rightarrow \mathbb{R}$ be of bounded variation and supported in $\hat{\Omega}_x$, $g : \mathbb{R} \rightarrow \mathbb{R}$ lying in $W^{1,\infty}(\mathbb{R})$ non-decreasing, g' is compactly supported in $\hat{\Omega}_x$ and $\text{range}(g) \supset \Omega_x$. Suppose f_ε and g_ε are continuous piecewise linear functions, and f_ε is of the form $f_\varepsilon = \sum_{i=1}^N c_i \rho_\varepsilon(x - x_i)$ for some grid points $\mathcal{X} = \{x_i\}_{i=1}^N \subset \hat{\Omega}_x$ such that $|f_\varepsilon|_{TV(\hat{\Omega}_x)} \leq |f|_{TV(\hat{\Omega}_x)}$.*

Define the function $f_\varepsilon \circ^+ g_\varepsilon \in C(\Omega_x) \cap P_1(\Omega_x)$ as

$$(4.10) \quad f_\varepsilon \circ^+ g_\varepsilon(x) := \sum_{i=1}^N c_i \rho_\varepsilon(x - g_\varepsilon(x_i)).$$

Then we have for parameter $\varepsilon > 0$ sufficiently small depending on the grid width,

$$(4.11) \quad \begin{aligned} & \|f \circ g^+ - f_\varepsilon \circ^+ g_\varepsilon\|_{L^1(\Omega_x)} \\ & \leq \|g'\|_{L^\infty(\hat{\Omega}_x)} \|f - f_\varepsilon\|_{L^1(\hat{\Omega}_x)} \\ & \quad + |f|_{TV(\hat{\Omega}_x)} \left[\left(1 + \|g'\|_{L^\infty(\hat{\Omega}_x)} \right) \|\rho - \rho_\varepsilon\|_{L^1(\mathbb{R})} + \|g - g_\varepsilon\|_{L^\infty(\mathcal{X})} \right]. \end{aligned}$$

In the special case $f \in P_0(\hat{\Omega}_x) \cap BV(\hat{\Omega}_x)$ the inequality reduces to

$$(4.12) \quad \begin{aligned} & \|f \circ g^+ - f_\varepsilon \circ^+ g_\varepsilon\|_{L^1(\Omega_x)} \\ & \leq |f|_{TV(\hat{\Omega}_x)} \left(\|\rho - \rho_\varepsilon\|_{L^1(\mathbb{R})} + \|g - g_\varepsilon\|_{L^\infty(\mathcal{X})} \right). \end{aligned}$$

Proof. See Appendix B.2. □

Although the inverse-bias trick might appear to apply solely in the single dimensional setting, it extends to multiple dimensions when one views the neural network approximation as a superposition of ridge functions, for instance via the Radon transform [57, 35, 7, 68, 69]. Close connections have been made to neural networks, e.g. see [11, 61, 81].

4.2 LRNR approximation of transported subspaces In this section, we will show that a 2-layer version of LRNR, a simple special case of the general definition of LRNRs introduced in Sec. 3, is able to approximate any transported subspace. The rank of the approximating LRNR is equivalent to the dimension of the transported subspace.

Example 4.4 (A 2-layer version of LRNR). Suppose we are given

(i) a set of vectors

$$(4.13) \quad \begin{aligned} \mathbb{U}_r^1 &= (U_i^1)_{i=1}^r \subset \mathbb{R}^M, \quad \mathbb{U}_r^2 = (U_i^2)_{i=1}^r \subset \mathbb{R}^M, \quad \mathbb{V}_r^1 = (V_i^1)_{i=1}^r \subset \mathbb{R}^M, \\ \mathbb{V}_r^2 &= (V_i^2)_{i=1}^r \subset \mathbb{R}, \end{aligned}$$

so that the dimensions are at most $r \in \mathbb{N}$, that is,

$$(4.14) \quad \dim \mathbb{U}_r^\ell, \dim \mathbb{V}_r^\ell \leq r, \quad \text{for } \ell = 1, 2,$$

(ii) coefficient sets $C = (C_1, C_2), D = (D_1, D_2)$ both in \mathbb{R}^{2r} .

Then let us denote,

$$(4.15) \quad \mathbb{W}_r := (C_1 \cdot \mathbb{U}_r^1) \times (C_2 \cdot \mathbb{U}_r^2), \quad \mathbb{B}_r := (D_1 \cdot \mathbb{V}_r^1) \times (D_2 \cdot \mathbb{V}_r^2).$$

The corresponding LRNR H_r of rank r , d.o.f K , width M , depth $L = 2$ is given as the family of functions

$$(4.16) \quad H_r := \left\{ h \in P_1(\mathbb{R}) \cap C(\mathbb{R}) \mid \begin{array}{l} h(x) = w_2 \cdot \sigma(w_1 x + b_1) + b_2, \\ (w_1, w_2) \in \mathbb{W}_r, (b_1, b_2) \in \mathbb{B}_r \end{array} \right\}.$$

We will denote by $h(\gamma, \theta)$ the member $h \in H_r$ whose coefficients are $(\gamma, \theta) \in C \times D$.

We now show that every transported subspace \bar{H}_{r-1} can be uniformly approximated by a LRNR H_r with comparable rank. LRNR needs one more rank due to a technicality in representing the jump function using (4.9).

THEOREM 4.5. *For each transported subspace \bar{H}_{r-1} with basis functions in Ψ_{r-1} taking on the form*

$$(4.17) \quad \psi_i(x) = \sum_{j=1}^{N_i} c_{ij} \rho(x - x_{ij}), \quad i = 1, \dots, r,$$

a pair of coefficient sets (A, B) , and a given parameter $\varepsilon > 0$, there exists a LRNR H_r that has d.o.f $K \lesssim \sum_{i=1}^r N_i$, width $M \sim K$, and depth $L = 2$, along with coefficient sets C, D and an affine map $\mu : A \times B \rightarrow C \times D$ mapping $\mu(\alpha, \beta) = (\gamma, \theta)$, such that the members $\bar{h}(\alpha, \beta) \in \bar{H}_{r-1}$ and $h(\gamma, \theta) \in H_r$ satisfy

$$(4.18) \quad \|\bar{h} - h\|_{L^1(\Omega_x)} \leq \left(\sum_i |\psi_i|_{TV(\hat{\Omega}_x)} \right) \left(\sup_{\beta \in B} \|\beta\|_\infty \right) \|\rho - \rho_\varepsilon\|_{L^1(\Omega_x)}.$$

Proof. See Appendix B.3. \square

The parameter error can be made arbitrarily small by increasing the width K , so \bar{H}_{r-1} is in the L^1 closure of H_r . Note also that the total variation norm can be relaxed to a Besov norm, although we will not pursue the details here.

4.3 LRNR approximation of classical solutions Now that we have shown that there are LRNR approximations of transported subspaces (Thm. 4.5), it is natural to ask whether the classical solution can be approximated uniformly well by a LRNR. We show that this is indeed the case.

THEOREM 4.6. *For the classical solution*

$$(4.19) \quad u(t) = u_0 \circ X^{-1}(\cdot, t), \quad t \in \Omega_t, \quad u_0 \in C^1(\Omega_x) \cap \mathcal{U},$$

there is a LRNR H_r with rank $r = 3$, d.o.f K , width $M \sim K$, and depth $L = 2$ such that, for coefficients $\gamma(t), \theta(t)$ that are linear or constant functions of t , the member $h(t) = h(\gamma(t), \theta(t)) \in H_r$ achieves the uniform error

$$(4.20) \quad \|u(t) - h(t)\|_{L^1(\Omega_x)} \lesssim \frac{1}{K} |u_0|_{TV(\Omega_x)} (1 + T \|F''\|_{L^\infty(u_0(\Omega_x))} \|u_0'\|_{L^\infty(\Omega_x)}).$$

Proof. See Appendix B.5. \square

We remark here that the classical norm $\|u'_0\|_{L^\infty(\Omega_x)}$ can be avoided, as will become apparent in the results in the next section (Thm. 5.4). Its presence here is attributable to the separate approximation of the initial condition u_0 and the characteristic curves X , without taking into consideration the simplifications arising in their composition. Still, this result uses a straightforward approximation and demonstrates that, given sufficient width, the intrinsic low dimension can be exploited by LRNR.

We briefly emphasize again that while the transported subspace requires that its coefficient sets be admissible, the LRNR does not require similar constraints. The representation makes sense for any coefficients γ and θ , and this is a consequence of the inverse-bias trick.

5 LRNR approximation of entropy solutions Having constructed an efficient LRNR approximation of the classical solution, we turn our attention to the LRNR approximation of the entropy solution. As briefly discussed in the beginning of Sec. 4, there are important differences between the classical solution and the entropy solution. Let us explain how these differences introduce significant challenges in constructing the LRNR approximation.

Recall from Sec. 2 that we have introduced two new representations of the entropy solution, namely, one using the rarefied characteristics \hat{X} (2.25) and another using the relief characteristics \check{X} (2.32):

$$(5.1) \quad \begin{aligned} u_0 \circ X^{-1}(x, t) & \quad \text{classical characteristics,} \\ \hat{u}_0 \circ \hat{X}^+(x, t) & \quad \text{rarefied characteristics,} \\ \hat{u}_0 \circ \check{X}^+(x, t) & \quad \text{relief characteristics.} \\ & = \hat{u}_0 \circ (\hat{I} + t(F' \circ \hat{u}_0) + C_x \rho \circ (t - \lambda))^+ \end{aligned}$$

The rarefied characteristics \hat{X} is a direct generalization of the classical characteristics that allows representing shocks and rarefaction waves. It is monotone, thus the inverse-bias trick can still be applied directly to handle the left-inverse $(\cdot)^+$. However, as we discuss below, the rarefied characteristics are not in a compositional low rank form that is compatible with an efficient representation by LRNRs. On the other hand, the relief characteristics \check{X} do have a compositional low rank structure (as discussed in Sec. 3) that is compatible with LRNRs. However, it is not monotone and hence the left-inverse cannot be removed using the inverse-bias trick directly and an additional layer of approximation is required (see paragraphs following (4.7)).

Therefore, our goal here is to devise a LRNR approximation that agrees with the rarefied characteristics \hat{X} , while simultaneously exploiting the compositional low-rank structure of the relief characteristics \check{X} . We build a construction by decomposing the rarefied characteristics into sum of local-in-time contributions, and introduce a LRNR structure per each summand via the same technique used to for relief characteristics. This allows us to take advantage of the compositional structure while not necessarily maintaining monotonicity.

In this section we will address these challenges involved and construct an efficient LRNR approximation of the entropy solution. We first provide a broad outline in Sec. 5.1, then introduce various discretizations that gradually reveal the neural-network-like structure in Sec. 5.2 and Sec. 5.3, to finally work towards the main

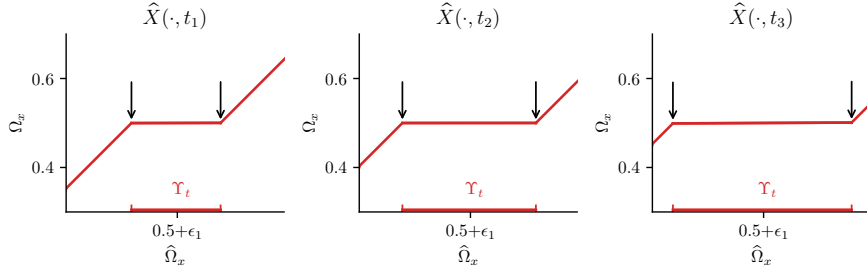


Fig. 5.1: The time evolution of the rarefied characteristics $\hat{X}(\cdot, t)$ for the stationary shock example in Fig. 2.4, zoomed into the region relevant to shock propagation. The constant interval (marked by Υ_t) expands over time $0 < t_1 < t_2 < t_3$. The two kinks at the endpoints (marked by two arrows) of this interval travel in opposite directions over time.

Thm. 5.4 in Sec. 5.4. Throughout, we refer the reader to Appendix A for a glossary of various approximations introduced in this section.

5.1 Outline of approach In this section, we will motivate and outline our general approximation approach. We begin by detailing the technical challenges mentioned in the introduction of this section. In light of the inverse-bias trick in Sec. 4.1, it might appear that the approximation of the entropy solution is now a simple matter of approximating the rarefied characteristics \hat{X} (2.22). Unfortunately, the rarefied characteristics manifold given by

$$(5.2) \quad \mathcal{M}_{\hat{X}} := \{\hat{X}(\cdot, t) : t \in \Omega_t\},$$

itself has a slowly decaying Kolmogorov n -width in the presence of shocks. For example, recall the stationary shock example from Fig. 2.4. Observe how the rarefied characteristics $\hat{X}(\cdot, t)$ evolves over time, as illustrated in Fig. 5.1. The constant region of $\hat{X}(\cdot, t)$ describing the shock expand with time, according to the Rankine-Hugoniot condition, and this leads to kinks that travel across the domain $\hat{\Omega}_x$. As a result, the n -width in L^2 -norm must be $\gtrsim n^{-3/2}$ [83, 60, 31, 72]. This is an obstruction to the strategy of finding a compositional reduced model directly, by using e.g. transported subspaces (Def. 4.2). In other words, there is now a slow decay in the n -width of *both* the solution manifold *and* the rarefied characteristics manifold.²

One natural question to ask is whether it is possible to construct compositional reduced models yet again, this time for the manifold of rarefied characteristics $\mathcal{M}_{\hat{X}}$. A low-rank structure is apparent in the relief characteristics \check{X} (2.31), in the superpositions of a few basis functions, as discussed in Sec. 3; see the diagram in (3.1). Still, we need care in introducing the shock-related jump term $\rho(\lambda(x) - t)$ that appears in the inner-most composition (2.31). In the relief characteristics, this term is used in conjunction with the left-inverse to replace the portions of the rarefied characteristic curves with constant regions. LRNRs are defined using ReLU activations so they

²To provide a succinct analogy: The classical characteristics are to the solution manifold, what the shock time function is to the rarefied characteristics manifold.

are continuous piecewise linear functions; as such, the jump discontinuity must be approximated carefully so that the low-rank compositional structure is preserved. We propose a LRNR approximation that satisfies these requirements, outlined as follows.

- We start with a continuous piecewise linear approximation of the rarefied characteristics with multivalued inverse (2.26),

$$(5.3) \quad \hat{X}_0(\cdot, t) \approx \sum_k c_k(t) \rho_\varepsilon(\cdot - x_k).$$

This approximation so far does not properly handle shocks.

- As discussed above, the LRNR approximation of shock propagation must be done carefully to preserve the compositional low rankness of the overall approximation and avoid the slow decay in the Kolmogorov width. We represent shocks (constant regions) by removing certain variations in the characteristics, emulating the relief characteristics while preserving continuous piecewise linearity and monotonicity. Roughly speaking, we achieve this by introducing a time-layered approximation so that slices of $\hat{X}_0(\cdot, t)$ are translated outside of the domain.

To maintain uniform error between \hat{X} and this approximation, it is necessary that the slice that is being translated to the right does so quickly and is small in amplitude. A key observation that makes this possible is that, in the approximation (5.3), there is a freedom in constructing the coefficients (c_k). Without adding to the number of coefficients, one may restructure the coefficients so that the approximation is rewritten as a sum of the slices (η_k). With some simplifications, one writes

$$(5.4) \quad \hat{X}_0(\cdot, t) \approx \hat{I}(\cdot) + tv(\cdot) + \sum_k t \eta_k(\cdot), \quad \|t \eta_k\|_{L^\infty(\hat{\Omega}_x)} \lesssim \varepsilon.$$

Note that this approximates the multi-valued inverse and does not properly represent shocks.

- We modify the above approximation to represent shocks, by an appropriate removal of slice terms to mimick the expanding constant regions of \hat{X} . That is, we write

$$(5.5) \quad \hat{X}(\cdot, t) \approx \pi(\cdot, t) \approx \hat{I}(\cdot) + tv(\cdot) + \sum_{\substack{\text{partial sum} \\ \text{over } k}} t \eta_k(\cdot), \quad \|t \eta_k\|_{L^\infty(\hat{\Omega}_x)} \lesssim \varepsilon,$$

where π denotes a piecewise linear approximation of \hat{X} we will construct in the following section. Now, we have an appropriate approximation of the rarefied characteristics, thereby representing shocks properly. However, the partial summation over k is not a compositional operation, so it is not yet amenable to efficient LRNR approximations.

- Now each slice η_k can be removed from the domain using the inverse-bias trick devised for (2.31): This amounts to inserting an approximation of the term $\rho(t - \lambda(x))$ into the bias,

$$(5.6) \quad \hat{X}(\cdot, t) \approx \bar{\pi}(\cdot, t) \approx \hat{I}(\cdot) + tv(\cdot) + \sum_k t \eta_k(\cdot - C_x \rho_\varepsilon(t - \lambda(x_k))), \quad x_k \in \text{supp } \eta_k,$$

with C_x sufficiently large (2.31). Finally, the $\bar{\pi}$ is a continuous piecewise linear approximation that is efficiently representable in the form of a LRNR that we will construct below. This approximation is not monotone, but it is still well-defined where the approximation is not monotone and is compatible with the inverse-bias trick, as an approximation to \hat{X} (Sec. 4.1 and Lem. 4.3). Note that this approximation has the compositional structure of relief characteristics; the bias term $C_x \rho_\varepsilon(t - \lambda(x_k))$ plays the role of the term $C_x \rho(t - \lambda(x))$ in \tilde{X} (5.1). Whenever $|t - \lambda(x_k)| \lesssim \varepsilon$, i.e. approximately the time when the characteristic curve emanating from x_k has entered into the shock, a portion of the characteristic information η_k is moved outside of the domain $\hat{\Omega}_x$ with speed $\sim 1/\varepsilon$.

We present our construction as follows. In Sec. 5.2, we derive a time-layered approximation of rarefied characteristics \hat{X} that is valid for short time intervals, then in Sec. 5.3 we construct a discretization of the form (5.6), then finally in Sec. 5.4 we present the LRNR approximation result.

In the following sections, we will make use of a few special symbols to denote functions, due to the intuitive relation between their shape and the referenced function: \vdash , \dashv , π , and $\bar{\pi}$ are standard symbols used throughout the mathematics literature for various purposes.³

We close this outline with the remark that the use of a threshold function in (5.6) shares a similar theme with TSI [83], transport reversal [70], or FTR [44].

5.2 A time-layered approximation of the rarefied characteristics We first introduce an approximation of $\hat{X}(x, t)$ (2.22) that is accurate for a given time interval. This approximation will be uniformly accurate, with the error controlled by the number of degrees of freedom depending on the complexity of u_0 and the flux function F .

To simplify our discussion, let us define two functions we call *left shock endpoint* and *right shock endpoint* of a shock containing the point x at time t ,

$$(5.7) \quad \vdash, \dashv : \{(x, t) \mid x \in \Upsilon_t, t \in \Omega_t\} \rightarrow \hat{\Omega}_x,$$

which are given respectively by

$$(5.8) \quad \vdash(x, t) := \inf_z \{[z, x] \in \Upsilon_t\}, \quad \text{and} \quad \dashv(x, t) := \sup_z \{[x, z] \in \Upsilon_t\}.$$

Note that these endpoints can represent arbitrary number of shocks; the ranges $\vdash(\Upsilon_t, t)$ and $\dashv(\Upsilon_t, t)$ yield left and right endpoints of *all* shocks that have formed up to time t . For the points $x \in \Upsilon_t$, that is, the points in $\hat{\Omega}_x$ whose subsequent characteristic curves go into the shock at time t , the function values $\vdash(x, t)$ and $\dashv(x, t)$ are the left and right most end points of the maximal interval containing the point that are in the shock at the time.

Since $\hat{X}(\cdot, t)$ is continuous and it is constant in the interval $[\vdash(x, t), \dashv(x, t)]$,

$$(5.9) \quad \hat{X}(\vdash(x, t), t) = \hat{X}(\dashv(x, t), t) = \hat{X}(z, t), \quad z \in [\vdash(x, t), \dashv(x, t)].$$

³These symbols can be interpreted as Hangul letters, which makes them pronounceable as *a*, *eo*, *jieut*, and *chieut*, respectively [80].

Furthermore, since we assumed our initial condition was in $\bar{\mathcal{U}}$ (2.3), and our problem is homogeneous (2.1),

$$(5.10) \quad \# \left(\vdash(\hat{\Omega}_x, t) \right) = \# \left(\dashv(\hat{\Omega}_x, t) \right) \leq \# \left(\{x \in \hat{\Omega}_x : u_0(x_-) \neq u_0(x_+)\} \right),$$

where the RHS is the number of jumps in the initial condition u_0 , and $\#(\cdot)$ denotes the cardinality of the set. For such an initial condition, the number of jumps does not increase [76].

For a fixed $x \in \hat{\Omega}_x$, the shock endpoints $\vdash(x, \cdot)$ and $\dashv(x, \cdot)$ are strictly decreasing and increasing with t , respectively, that is,

$$(5.11) \quad \text{if } 0 \leq t_1 < t_2 \leq T \quad \text{then} \quad \vdash(x, t_2) < \vdash(x, t_1) \text{ and } \dashv(x, t_1) < \dashv(x, t_2),$$

since the characteristic curves always enter into the shock, not vice versa.

Due to the differential equations that yield this evolution (2.22), the endpoints \vdash, \dashv are piecewise continuously differentiable with respect to t , except at finitely many points in Ω_t .

Let $k \in \mathbb{N}$, $t_k \in \Omega_t$ with $t_k \leq t_{k+1}$, then define the indexed functions we call *time-layered approximations* $\Xi_k \in C(\hat{\Omega}_x \times \Omega_t)$ of \hat{X} ,

$$(5.12) \quad \Xi_k(x, t) := \hat{I}(x) + t v_k(x),$$

where v_k is defined as the continuous function

$$(5.13) \quad v_k(x) := \begin{cases} (F' \circ \hat{u}_0)(x) & \text{if } \lambda(x) > t_k, \\ (F' \circ \hat{u}_0)(\vdash(x, t_k)) & \text{if } \lambda(x) \leq t_k. \end{cases}$$

Note that $v_k(x)$ is constant in each connected component of the domain $\Upsilon_{t_k} = \{x \in \hat{\Omega}_x : \lambda(x) \leq t_k\}$, and that v_k can be defined using \dashv in place of \vdash . The function Ξ_k satisfies the following estimates.

LEMMA 5.1. *For $t \in [t_k, t_{k+1}]$ we have the estimates,*

$$(5.14) \quad \|\hat{X}(\cdot, t) - \Xi_k(\cdot, t)\|_{L^\infty(\hat{\Omega}_x)} \leq |u_0|_{TV(\Omega_x)} \|F''\|_{L^\infty(u_0(\Omega_x))} |t_{k+1} - t_k|,$$

$$(5.15) \quad |\Xi_k(\cdot, t)|_{TV(\hat{\Omega}_x)} \leq 1 + T |u_0|_{TV(\Omega_x)} \|F''\|_{L^\infty(u_0(\Omega_x))}.$$

Proof. See Appendix B.4. \square

Next, suppose we let $(t_k)_{k=1}^K$ be a uniform grid over time domain Ω_t ,

$$(5.16) \quad t_k := (k-1) \frac{T}{K},$$

then we have our time-layered approximation Ξ_k which satisfies the uniform estimate

$$(5.17) \quad \|\hat{X}(\cdot, t) - \Xi_k(\cdot, t)\|_{L^\infty(\hat{\Omega}_x)} \leq \frac{T}{K} |u_0|_{TV(\Omega_x)} \|F''\|_{L^\infty(u_0(\Omega_x))}.$$

See Fig. 5.2 for an illustration of this approximation.

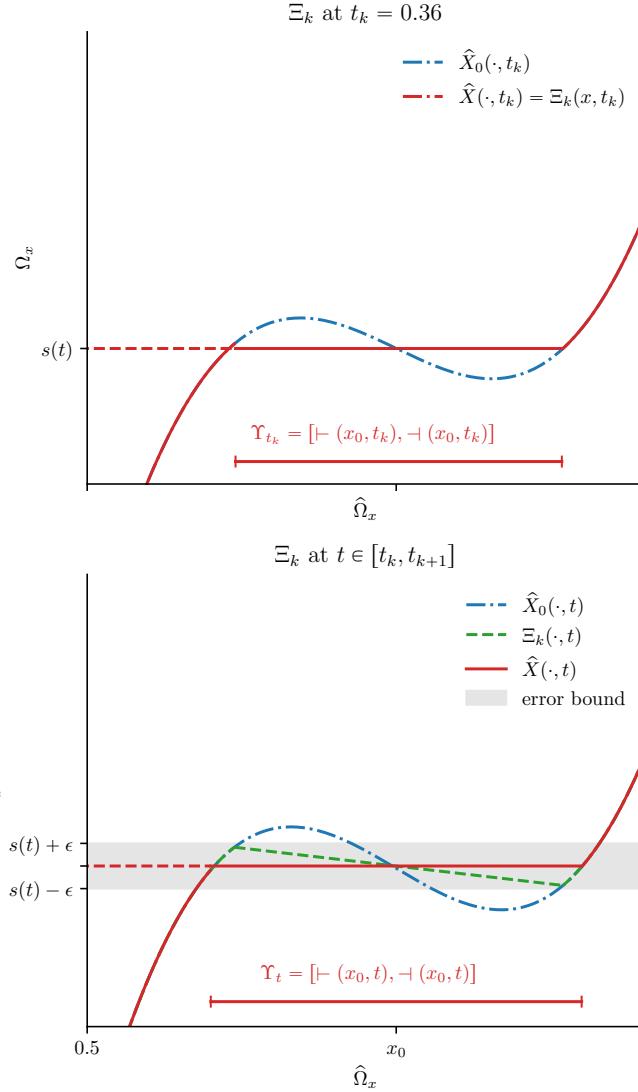


Fig. 5.2: An illustration of time-layered approximation Ξ_k (5.12) immediately after shock formation, compared with the rarefied characteristics with multivalued inverse \hat{X}_0 and the rarefied characteristics \hat{X} . At uniform grid times t_k (5.16) the $\Xi_k(\cdot, t_k) = \hat{X}(\cdot, t_k)$, however, as the time is evolved forward $\Xi_k(\cdot, t)$ is different from $\hat{X}(\cdot, t_k)$ in general, and the difference is within the ϵ error bound.

5.3 The spatial discretization of time-layered approximation Now we introduce the appropriate spatial discretization of the time-layered approximations Ξ_k (5.12) that we have constructed in the previous section.

Let us introduce a notation for a constant that will appear repeatedly,

$$(5.18) \quad C_{u_0, T, F} := T |u_0|_{TV(\Omega_x)} \|F''\|_{L^\infty(u_0(\Omega_x))}.$$

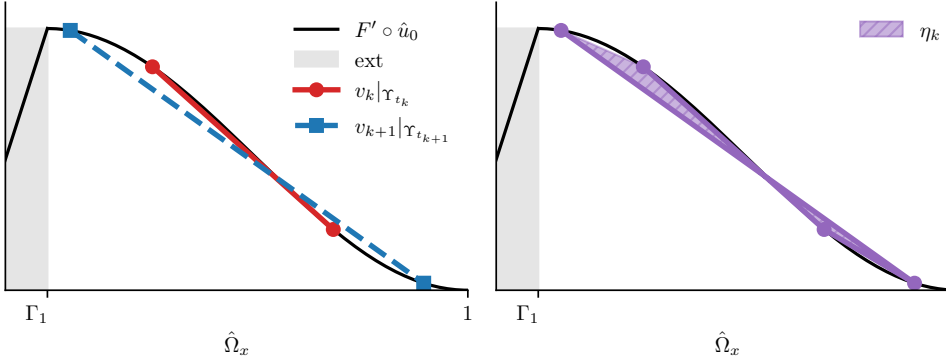


Fig. 5.3: An illustration of the interpolant η_k (5.21) along with the functions v_k and v_{k+1} (5.13). The thin slice η_k is plotted to the right.

In the following, we will make use of the estimates (5.14) and (5.15) in Lem. 5.1, and the uniform time grid t_k with grid size K (5.16).

Because of the TV bound (5.15), there is an adaptive spatial grid $(z_i)_{i=1}^K$ over $\hat{\Omega}_x$ on which we have continuous piecewise linear approximations $\pi_k(\cdot, t) \in C(\hat{\Omega}_x \times \Omega_t) \cap P_1(\hat{\Omega}_x \times \Omega_t)$ of $\Xi_k(\cdot, t)$ satisfying

$$(5.19) \quad \|\Xi_k(\cdot, t) - \pi_k(\cdot, t)\|_{L^\infty(\hat{\Omega}_x)} \leq \frac{1}{K} (1 + C_{u_0, T, F}), \quad \text{for } k = 1, \dots, K-1.$$

We refer the reader to [23] for the details of the estimate and the grid construction. Note here that we have chosen the size of the adaptive grid to equal the size K of the time grid. Furthermore, we choose π_k so that it is an interpolant that satisfies

$$(5.20) \quad \pi_k(z_i, t_k) = \begin{cases} \hat{X}_0(z_i, t_k) & \text{for } z_i \in \hat{\Omega}_x \setminus \Upsilon_{t_k}, \\ \hat{X}(z_i, t_k) & \text{for } z_i \in \Upsilon_{t_k}. \end{cases}$$

We have now obtained the interpolants (π_k) , and next we wish to exploit the fact that these interpolants are closely related to each other across the index k . They interpolate (Ξ_k) each in the form (5.12) containing the functions (v_k) . Observe that these functions approximate $F' \circ \hat{u}_0$ in $\hat{\Omega}_x \setminus \Upsilon_{t_k}$. Since (v_k) each approximate the same spatial function, it is possible to construct an approximation of (Ξ_k) for all k simply by reorganizing the point values of (π_k) by adding or removing the differences $(v_{k+1} - v_k)$. We do this by introducing a continuous piecewise linear interpolant of these differences.

For each index k , let $\eta_k \in C(\hat{\Omega}_x) \cap P_1(\hat{\Omega}_x)$ be an approximation of $v_{k+1} - v_k$ on the grid (z_i) , specifically,

$$(5.21) \quad \eta_k(z_i) = \frac{1}{t_{k+1}}(\pi_{k+1}(z_i, t_k) - \hat{I}(z_i)) - \frac{1}{t_k}(\pi_k(z_i, t_k) - \hat{I}(z_i)) \quad i = 0, 1, \dots, K-1.$$

Then η_k is nonzero only at the grid points $(z_i)_{i=1}^K$ that lie in $\Upsilon_{t_{k+1}} \cup \Upsilon_{t_k}$. See Fig. 5.3 for an illustration.

A quick calculation yields for $t \in [t_k, t_{k+1}]$,

$$\begin{aligned}
& \|t\eta_k\|_{L^\infty(\hat{\Omega}_x)} \\
(5.22) \quad & \leq \|t\eta_k - t(v_{k+1} - v_k)\|_{L^\infty(\hat{\Omega}_x)} + \|t(v_{k+1} - v_k)\|_{L^\infty(\hat{\Omega}_x)} \\
& \leq t\|\eta_k - (v_{k+1} - v_k)\|_{L^\infty(\hat{\Omega}_x)} + \|\Xi_k - \Xi_{k+1}\|_{L^\infty(\hat{\Omega}_x)} \leq \frac{4C_{u_0,T,F}}{K},
\end{aligned}$$

due to (5.14) and (5.19).

Next, let us set the function $\pi : \hat{\Omega}_x \times \Omega_t \rightarrow \mathbb{R}$ which is continuous piecewise linear in space but only piecewise linear in time. Let $\pi_K(x, t) := \hat{I}(x) + \frac{t}{T}(\pi_K(x, t_K) - \hat{I}(x))$ and

$$(5.23) \quad \pi(x, t) := \pi_K(x, t) + t \left[\sum_{k:t < t_k} \eta_k(x) \right]$$

for which we have the estimate,

$$\begin{aligned}
& \|\hat{X}(\cdot, t) - \pi(\cdot, t)\|_{L^\infty(\hat{\Omega}_x)} \\
& \leq \|\hat{X}(\cdot, t) - \Xi_k(\cdot, t)\|_{L^\infty(\hat{\Omega}_x)} \\
(5.24) \quad & \quad + \|\Xi_k(\cdot, t) - \pi_k(\cdot, t_k)\|_{L^\infty(\hat{\Omega}_x)} + \|\pi_k(\cdot, t_k) - \pi(\cdot, t)\|_{L^\infty(\hat{\Omega}_x)} \\
& \leq \frac{C_{u_0,T,F}}{K} + \frac{1 + C_{u_0,T,F}}{K} + \frac{4C_{u_0,T,F}}{K} \\
& \leq \frac{1 + 6C_{u_0,T,F}}{K}.
\end{aligned}$$

Finally, define the fully continuous piecewise linear $\bar{\pi} \in C(\hat{\Omega}_x \times \Omega_t) \cap P_1(\hat{\Omega}_x \times \Omega_t)$,

$$(5.25) \quad \bar{\pi}(x, t) := \pi_K(x, t) + t \sum_{k=0}^{K-1} \eta_k \left(x - C_x \sigma \left(\frac{K}{T}(t - t_k) \right) \right),$$

for a constant $C_x \geq |\Omega_x|$. Notice how the summation indices are over all k : Essentially, through the modification $x \mapsto x - C_x \sigma \left(\frac{K}{T}(t - t_k) \right)$ we are emulating the partial sum over k in (5.23) by quickly translating the η_k terms outside of the spatial domain $\hat{\Omega}_x$.

We briefly digress to point out that this approximation is the implementation of (5.6). One can show that the uniform time grid-point t_k appearing in the inner-most argument is approximately $\lambda(z)$ for some $z \in \text{supp } \eta_k$ up to ε error. This fact, together with (5.22), implies that $\bar{\pi}$ is indeed approximated by the expression

$$(5.26) \quad \bar{\pi}(x, t) \approx \pi_K(x, t) + t \sum_{k=0}^{K-1} \eta_k \left(x - C_x \sigma \left(\frac{K}{T}(t - \lambda(z_{i_k})) \right) \right),$$

in which $z_{i_k} \in (z_i)_{i=1}^K$ is any grid point picked to be in $\text{supp } \eta_k$. Noting that η_k are piecewise linear functions that can be approximated by a linear combination of functions $\rho_\varepsilon(\cdot - x_k)$ appearing in (5.6), and that $K/T \sim 1/\varepsilon$, one sees that $\bar{\pi}$ indeed approximates \hat{X} in the manner described above. The approximation is thus an analogue of the relief characteristics \check{X} described above (2.31); it omits the part of

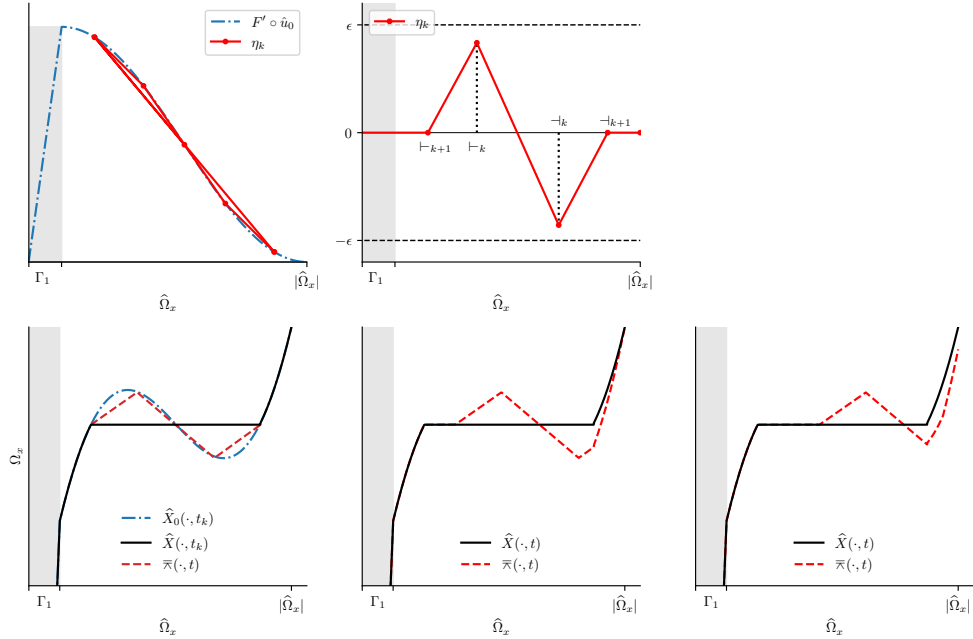


Fig. 5.4: A diagram depicting the approximation by $\bar{\pi}(x, t)$. The term $F' \circ \hat{u}_0$ in the rarefied characteristics with multivalued inverse \hat{X}_0 along with the interpolant η_k (5.21) are shown in the upper left plot. The interpolant η_k along with the left and right shock endpoints \vdash, \dashv at times t_k and t_{k+1} are shown in the upper center plot. The three lower plots show a movie illustrating the evolution of $\bar{\pi}(x, t)$ starting at time $t = t_k$. The thin interpolant η_k representing a tiny perturbation of the characteristic curves, is moving out of the spatial domain to the right, traveling quickly outside the domain.

the characteristics that has entered the shock, simply by moving the data out of the domain, using a certain thresholding of the shock-time function in conjunction with the inverse-bias trick. See Fig. 5.4 for a depiction of how $\bar{\pi}$ approximates the constant region representing shocks.

We will next prove a uniform error estimate for $\bar{\pi}$.

LEMMA 5.2. *The approximation $\bar{\pi} \in C(\hat{\Omega}_x \times \Omega_t) \cap P_1(\hat{\Omega}_x \times \Omega_t)$ defined above in (5.25) satisfies*

$$(5.27) \quad \|\hat{X}(\cdot, t) - \bar{\pi}(\cdot, t)\|_{L^\infty(\hat{\Omega}_x)} \lesssim \frac{1}{K} \left(1 + T |u_0|_{TV(\Omega_x)} \|F''\|_{L^\infty(u_0(\Omega_x))} \right).$$

Proof. See Appendix B.6. \square

Based on the continuous piecewise linear analogue $\bar{\pi}$ of the rarefied characteristics, we now construct an approximation of the entropy solution u . We will make use of known approximations of u (see, e.g. [19]): There is an entropy solution \bar{u} with piecewise constant initial datum $\bar{u}_0 \in \bar{\mathcal{U}}$ satisfying

$$(5.28) \quad \|u(\cdot, t) - \bar{u}(\cdot, t)\|_{L^\infty(\Omega_x)} \lesssim \frac{1}{K} |u_0|_{TV(\Omega_x)}, \quad t \in \Omega_t.$$

Let \hat{u}_0 be the extended initial condition of such \bar{u}_0 constructed as in (2.20). Let $\hat{u}_{0\varepsilon}$ be its approximation (see, e.g. [23]) of the form

$$(5.29) \quad \hat{u}_{0\varepsilon}(x) = \sum_{i=1}^K \hat{u}_{0,i} \rho_\varepsilon(x - x_i),$$

that satisfies the error bound

$$(5.30) \quad \|\hat{u}_0 - \hat{u}_{0\varepsilon}\|_{L^1(\hat{\Omega}_x)} \lesssim \frac{1}{K} |u_0|_{TV(\Omega_x)}.$$

Furthermore, let $\bar{\pi}$ be the approximation constructed above (5.25) for the solution \bar{u} .

THEOREM 5.3. *Let u be the entropy solution to the scalar conservation law (2.1). Then for given $\hat{u}_{0\varepsilon}$ and $\bar{\pi}$ as above and $\varepsilon = 1/K$,*

$$(5.31) \quad \bar{h}(x, t) := \hat{u}_{0\varepsilon} \circ^+ \bar{\pi}(x, t) = \sum_{i=1}^K c_i \rho_\varepsilon(x - \bar{\pi}(x_i, t))$$

approximates the entropy solution u with the error estimate

$$(5.32) \quad \begin{aligned} & \|u(\cdot, t) - \bar{h}(\cdot, t)\|_{L^1(\Omega_x)} \\ & \lesssim \frac{1}{K} |u_0|_{TV(\Omega_x)} \left(1 + |u_0|_{TV(\Omega_x)} \right) \left(1 + T \|F''\|_{L^\infty(u_0(\Omega_x))} \right). \end{aligned}$$

Proof. See Appendix B.7. \square

The major issues identified in the introduction of this section are the monotonicity and the low rank compositional structure. The final approximation $\bar{\pi}$ of the rarefied characteristics is not necessarily monotone but sufficiently accurate, allowing the approximate version of the inverse-bias trick via Lem. 4.3. Observe how in (5.25) one sees that it has a low rank compositional structure reminiscent of the relief characteristics. This will form the foundation for constructing the LRNR approximation in Thm. 5.4 below.

The approximation error in (5.32) scales as $\sim K^{-1}$ and the constants depend only on the initial condition and the flux function. It is important to note that this rate implies that our construction is not a naïve space-time approximation, for which the error would scale with the d.o.f $\sim K^{-\frac{1}{2}}$.

Let us discuss the number of operations needed to evaluate the approximation \bar{h} (5.31) at points in the space-time domain. At initial time, to evaluate $\bar{\pi}(x_i, t)$ for $i = 1, \dots, K$, one needs the evaluation of $\hat{I}(x_i), v_K(x_i)$, which requires $\mathcal{O}(K)$ operations, so one evaluation of $h(x, 0)$ requires $\mathcal{O}(K)$ work. Then, to evaluate $h(\bar{x}_p, 0)$ for a grid $(\bar{x}_p)_{p=1}^K \subset \Omega_x$, $\mathcal{O}(K^2)$ work is needed. Then, to evaluate $h(\bar{x}_p, t_k)$ on the uniform time-grid t_k , one marches forward in time: At each time t_k the evaluation t_{k+1} can be obtained by sweeping through the spatial grid once, and each update costs $\mathcal{O}(1)$ for each \bar{x}_i , resulting in $\mathcal{O}(K)$ work for each time-update, by only adjusting one term in the sum appearing in the definition of $\bar{\pi}$ in (5.25). Thus, one can evaluate the piecewise linear approximation \bar{h} (5.31) at a space-time grid of size $\sim K^2$ using $\mathcal{O}(K^2)$ workload. This amounts to $\mathcal{O}(1)$ work for per space-time grid point.

Moreover, in this space-time approximation, the temporal approximation is trivial, due to the explicit linear time dependence as clearly seen in (5.25).

5.4 The LRNR approximation of compositional form We now prove that a LRNR construction can implement the approximation from the previous section.

THEOREM 5.4. *There is a LRNR H_r with rank $r = 2$, d.o.f K , width $\sim K^2$, and depth $L = 5$, such that for the solution to (2.1) with initial condition $u_0 \in \mathcal{U}$ at each time $u(t) := u(\cdot, t)$ there is a $h(t) := h(\gamma(t), \theta(t)) \in H_r$ with the approximation error*

$$(5.33) \quad \|u(t) - h(t)\|_{L^1(\Omega_x)} \lesssim \frac{1}{K} |u_0|_{TV} (1 + |u_0|_{TV}) (1 + T \|F''\|_{L^\infty(u_0(\Omega_x))}).$$

where the coefficients $\gamma(t), \theta(t)$ are linear or constant functions of t .

Proof. See Appendix B.8. \square

Note that neither the rank r nor the number of layers L depends on the initial condition. This result shows there is an upper bound on a kind of “nonlinear width” as described by the number of coefficients r and the number of layers L , namely the tuple $(r, L) = (2, 5)$ associated with the entropy solutions of the scalar conservation law (2.1) regardless of the complexity of the initial data or the shock topology structure.

Acknowledgements The authors thank Randall J. LeVeque for helpful discussions, and also thank Ari Stern for suggesting the term *shock time function*. Part of this work was done while D.R. was enjoying the hospitality of the International Research Institute of Disaster Science (IRIDeS) at Tohoku University through an invitation from Kenjiro Terada, supported by Invitational Fellowship Program for Collaborative Research with International Researcher (FY2023).

Appendix A. Glossary of definitions and relations.

Formulations of the entropy solution (Sec. 2).

A-1. u entropy solution (Sec. 2.1)

A-2. u_0 initial condition to the entropy solution (Sec. 2.1)

A-3. ξ mapping for similarity solution (2.9)

A-4. X characteristic curves (2.5)

$$(2.11) \quad u(x, t) = \begin{cases} u_0(X^+(x, t)) & (x, t) \in \Omega \setminus \mathcal{R} \\ (F')^{-1}(\xi(x, t)) & (x, t) \in \mathcal{R} \end{cases}$$

A-5. \hat{u}_0 an extension of the initial condition u_0 (2.20)

A-6. \hat{X} rarefied characteristic curves (2.22)

$$(2.25) \quad u(x, t) = \hat{u}_0 \circ \hat{X}^+(x, t) \quad (x, t) \in \Omega_x$$

A-7. \hat{X}_0 rarefied characteristics with multivalued inverse

$$(2.26) \quad \hat{X}_0(x, t) := \hat{I}(x) + t(F' \circ \hat{u}_0)(x) \quad (\text{where } \hat{I} \text{ is given in (2.23)})$$

A-8. $\rho = \mathbf{1}_{\mathbb{R}_+}$ threshold function

A-9. λ shock time function (Sec. 2.3)

A-10. \check{X} relief characteristic curves (2.31)

$$(2.32) \quad u(x, t) = \hat{u}_0 \circ \check{X}^+(x, t) \quad (x, t) \in \Omega$$

Low rank neural representation (LRNR) (Sec. 3).

A-11. $h(x; W, B)$ feedforward neural network (Def. 3.2)

A-12. σ ReLU activation (Def. 3.2)

A-13. L depth of a neural network (Def. 3.2)

A-14. M width of a neural network (Def. 3.2)

A-15. H_r low rank neural representation of rank r (Def 3.3)

A-16. K degree of freedom of a LRNR (Def. 3.3)

A-17. $\mathbb{W}_r, \mathbb{B}_r$ low dimensional weights and biases

$$(3.16) \quad \mathbb{W}_r = \bigtimes_{\ell=1}^L (C^\ell \cdot \mathbb{U}_r^\ell) \subset \mathbb{W} \quad \mathbb{B}_r = \bigtimes_{\ell=1}^L (D^\ell \cdot \mathbb{V}_r^\ell) \subset \mathbb{B}$$

A-18. LRNR (Def. 3.3)

$$(3.17) \quad H_r = \{h(W, B) \mid W \in \mathbb{W}_r, B \in \mathbb{B}_r\}$$

Transported subspaces, inverse-bias trick, LRNR approximation of classical solutions (Sec. 4).

A-19. $\bar{H}_r := (B \cdot \Psi_r) \circ (A \cdot \Phi_r)^{-1}$ transported subspace (Def. 4.2)

A-20. ρ_ε continuous piecewise linear approximation to the threshold function (4.9)

A-21. Inverse-bias trick for $(f, g) \in B \cdot \Psi_r \times A \cdot \Phi_r$

$$(4.7) \quad f \circ g^{-1}(x) = c_0 + \sum_k c_k \rho(g^{-1}(x) - x_k) = c_0 + \sum_k c_k \rho(x - g(x_k))$$

A-22. $f_\varepsilon \circ^+ g_\varepsilon$ continuous (finitely) piecewise linear analogue of the inverse bias trick

$$(4.10) \quad f_\varepsilon \circ^+ g_\varepsilon(x) = \sum_{i=1}^N c_i \rho_\varepsilon(x - g_\varepsilon(x_i))$$

A-23. LRNR ($L = 2, r = 3$) approximation $h(t) \in H_r$ to the classical solution (Thm. 4.6)

$$(4.20) \quad \|u(t) - h(t)\|_{L^1(\Omega_x)} \lesssim \frac{1}{K} |u_0|_{TV(\Omega_x)} (1 + T \|F''\|_{L^\infty(u_0(\Omega_x))} \|u'_0\|_{L^\infty(\Omega_x)})$$

LRNR approximation the entropy solution (Sec. 5).

A-24. \vdash, \dashv left and right shock endpoints (5.8)

A-25. t_k uniform time-grid $t_k = (k-1)T/K$

A-26. Ξ_k time-layered approximation $\Xi_k(x, t) = \hat{I}(x) + t v_k(x)$ (5.12) for the time window $[t_k, t_{k+1}]$

$$(5.17) \quad \|\hat{X}(\cdot, t) - \Xi_k(\cdot, t)\|_{L^\infty(\hat{\Omega}_x)} \leq \frac{T}{K} |u_0|_{TV(\Omega_x)} \|F''\|_{L^\infty(u_0(\Omega_x))}$$

A-27. π_k spatial discretization of the time-layered approximation Ξ_k for the time window $[t_k, t_{k+1}]$ satisfying

$$(5.19) \quad \|\Xi_k(\cdot, t) - \pi_k(\cdot, t)\|_{L^\infty(\hat{\Omega}_x)} \leq \frac{1}{K} (1 + C_{u_0, T, F})$$

$$(5.20) \quad \pi_k(z_i) = \begin{cases} \hat{X}_0(z_i, t_k) & \text{for } z_i \in \hat{\Omega}_x \setminus \Upsilon_t \\ \hat{X}(z_i, t_k) & \text{for } z_i \in \Upsilon_t \end{cases}$$

A-28. η_k approximation of $v_{k+1} - v_k$ appearing inside Ξ_k (5.21) satisfying

$$(5.22) \quad \|t\eta_k\|_{L^\infty(\hat{\Omega}_x)} \leq \frac{4C_{u_0,T,F}}{K}$$

A-29. $\bar{\pi}$ continuous piecewise linear approximation of the rarefied characteristics \hat{X}

$$(5.27) \quad \|\hat{X}(\cdot, t) - \bar{\pi}(\cdot, t)\|_{L^\infty(\hat{\Omega}_x)} \lesssim \frac{1}{K} \left(1 + T |u_0|_{TV(\Omega_x)} \|F''\|_{L^\infty(u_0(\Omega_x))} \right)$$

A-30. $\hat{u}_{0\varepsilon}$ continuous piecewise approximation of the extended initial condition \hat{u}_0 (5.29)

A-31. \bar{h} continuous piecewise linear approximation $\bar{h}(x, t) := \hat{u}_{0\varepsilon} \circ^+ \bar{\pi}(x, t)$ (5.31) satisfying

$$(5.32) \quad \begin{aligned} & \|u(\cdot, t) - \bar{h}(\cdot, t)\|_{L^1(\Omega_x)} \\ & \lesssim \frac{1}{K} |u_0|_{TV(\Omega_x)} \left(1 + |u_0|_{TV(\Omega_x)} \right) \left(1 + T \|F''\|_{L^\infty(u_0(\Omega_x))} \right) \end{aligned}$$

A-32. LRNR ($L = 5, r = 2$) approximation $h(t) \in H_r$ to the entropy solution (Thm. 5.4)

$$(4.20) \quad \|u(t) - h(t)\|_{L^1(\Omega_x)} \lesssim \frac{1}{K} |u_0|_{TV} (1 + |u_0|_{TV}) (1 + T \|F''\|_{L^\infty(u_0(\Omega_x))})$$

Appendix B. Proofs of theorems and lemmas.

B.1 Proof of Lemma 2.1 The characteristics \hat{X} restricted to Ω_x by the expression $\hat{X}(\iota(x), t)$ satisfy the same differential equation as X so they necessarily agree,

$$(B.1) \quad \hat{X}^+(x, t) = \iota \circ X^+(x, t) \quad \text{for } (x, t) \in \Omega \setminus \mathcal{R}.$$

Otherwise if $(x, t) \in \mathcal{R}$, the expression yields the similarity solution: suppose $y \in \hat{\Omega}_x$ satisfies $x = \hat{I}(y) + tF' \circ \hat{u}_0(y)$ then one can show that $(x - \bar{\xi}(x, t))/t = F' \circ \hat{u}_0(y)$, implying $\hat{u}_0(y) = (F')^{-1}[(x - \bar{\xi}(x, t))/t]$. This agrees with the entropy solution (2.11).

B.2 Proof of Lemma 4.3 Let us define,

$$(B.2) \quad f_0(x) := \sum_{i=1}^N c_i \rho(x - x_i), \quad f_0 \circ^+ g_\varepsilon(x) := \sum_{i=1}^N c_i \rho(x - g_\varepsilon(x_i)).$$

By the triangle inequality, we have

$$(B.3) \quad \begin{aligned} \|f \circ g^+ - f_\varepsilon \circ^+ g_\varepsilon\|_{L^1(\Omega_x)} & \leq \|f \circ g^+ - f_0 \circ g^+\|_{L^1(\Omega_x)} \\ & + \|f_0 \circ g^+ - f_0 \circ^+ g_\varepsilon\|_{L^1(\Omega_x)} \\ & + \|f_0 \circ^+ g_\varepsilon - f_\varepsilon \circ^+ g_\varepsilon\|_{L^1(\Omega_x)}. \end{aligned}$$

For the first term,

$$(B.4) \quad \begin{aligned} \|f \circ g^+ - f_0 \circ g^+\|_{L^1(\Omega_x)} & = \int_{\Omega_x} |f(g^+(x)) - f_0(g^+(x))| \, dx \\ & = \int_{\hat{\Omega}_x} |f(y) - f_0(y)| |g'(y)| \, dy \\ & = \|g'\|_{L^\infty(\hat{\Omega}_x)} \|f - f_0\|_{L^1(\hat{\Omega}_x)}, \end{aligned}$$

then for the second term,

$$\begin{aligned}
& \|f_0 \circ g^+ - f_0 \circ^+ g_\varepsilon\|_{L^1(\Omega_x)} \\
&= \int_{\Omega_x} \left| \sum_{i=1}^N c_i \rho(x - g(x_i)) - \sum_{i=1}^N c_i \rho(x - g_\varepsilon(x_i)) \right| dx \\
(B.5) \quad &\leq \sum_{i=1}^N |c_i| \int_{\Omega_x} |\rho(x - g(x_i)) - \rho(x - g_\varepsilon(x_i))| dx \\
&\leq \left(\sum_{i=1}^N |c_i| \right) \|g - g_\varepsilon\|_{L^\infty(\mathcal{X})} \leq |f_0|_{TV(\hat{\Omega}_x)} \|g - g_\varepsilon\|_{L^\infty(\mathcal{X})}.
\end{aligned}$$

Next, we have that

$$\begin{aligned}
& \|f_0 \circ^+ g_\varepsilon - f_\varepsilon \circ^+ g_\varepsilon\|_{L^1(\Omega_x)} \\
&= \int_{\Omega_x} \left| \sum_{i=1}^N c_i \rho(x - g_\varepsilon(x_i)) - \sum_{i=1}^N c_i \rho_\varepsilon(x - g_\varepsilon(x_i)) \right| dx \\
(B.6) \quad &\leq \sum_{i=1}^N |c_i| \int_{\Omega_x} |\rho(x - g_\varepsilon(x_i)) - \rho_\varepsilon(x - g_\varepsilon(x_i))| dx \\
&\leq \frac{1}{2} \left(\sum_{i=1}^N |c_i| \right) \|\rho - \rho_\varepsilon\|_{L^1(\mathbb{R})} \leq |f_0|_{TV(\hat{\Omega}_x)} \|\rho - \rho_\varepsilon\|_{L^1(\mathbb{R})}.
\end{aligned}$$

Now $|f_0|_{TV(\hat{\Omega}_x)} \leq |f_\varepsilon|_{TV(\hat{\Omega}_x)} \leq |f|_{TV(\hat{\Omega}_x)}$ for ε sufficiently small, and further

$$\begin{aligned}
(B.7) \quad & \|f - f_0\|_{L^1(\hat{\Omega}_x)} \leq \|f - f_\varepsilon\|_{L^1(\hat{\Omega}_x)} + \|f_\varepsilon - f_0\|_{L^1(\hat{\Omega}_x)} \\
&\leq \|f - f_\varepsilon\|_{L^1(\hat{\Omega}_x)} + |f|_{TV(\hat{\Omega}_x)} \|\rho - \rho_\varepsilon\|_{L^1(\hat{\Omega}_x)}.
\end{aligned}$$

Putting together these inequalities,

$$\begin{aligned}
& \|f \circ g^+ - f_\varepsilon \circ^+ g_\varepsilon\|_{L^1(\Omega_x)} \\
(B.8) \quad &\leq |f|_{TV(\Omega_x)} (\|g - g_\varepsilon\|_{L^\infty(\mathcal{X})} + \|\rho - \rho_\varepsilon\|_{L^1(\mathbb{R})}) \\
&\quad + \|g'\|_{L^\infty(\hat{\Omega}_x)} (\|f - f_\varepsilon\|_{L^1(\hat{\Omega}_x)} + |f|_{TV(\hat{\Omega}_x)} \|\rho - \rho_\varepsilon\|_{L^1(\mathbb{R})}),
\end{aligned}$$

and the result follows upon rearranging the terms.

B.3 Proof of Theorem 4.5 We will first write each member $\bar{h} \in \bar{H}_{r-1}$ as a NN. Then we will write the collection of these NNs as a LRNR. Let $\bar{h} = f(\beta) \circ g(\alpha)^+$ and write $f(\beta)$ as

$$(B.9) \quad f(\beta) = \sum_i \beta_i \psi_i = \sum_{k=1}^K \bar{c}_k(\beta) \rho(\cdot - x_k),$$

for some coefficients $\bar{c}_k(\beta)$ that depend linearly on β , and $\mathcal{X} := \{x_k\}_{k=1}^K = \cup_i \{x_{ij}\}_{j=1}^{N_i}$. Recall that $g(\alpha) = \sum_{i=1}^r \alpha_i \phi_i$. Then, for corresponding continuous piecewise linear $f_\varepsilon(\beta)$ and $g_\varepsilon(\alpha)$, we have by Lem. 4.3,

$$\begin{aligned}
(B.10) \quad & \|f(\beta) \circ g(\alpha)^+ - f_\varepsilon(\beta) \circ^+ g_\varepsilon(\alpha)\|_{L^1(\Omega_x)} \\
&\leq |f(\beta)|_{TV(\hat{\Omega}_x)} (\|\rho - \rho_\varepsilon\|_{L^1(\mathbb{R})} + \|g(\beta) - g_\varepsilon(\beta)\|_{L^\infty(\mathcal{X})}).
\end{aligned}$$

By choosing g_ε to interpolate the point values $g_\varepsilon(\beta)(x_k) = g(\beta)(x_k)$ for $x_k \in \mathcal{X}$, the second term vanishes, yielding

$$(B.11) \quad \|f(\beta) \circ g(\alpha)^+ - f_\varepsilon(\beta) \circ^+ g_\varepsilon(\alpha)\|_{L^1(\Omega_x)} \leq |f(\beta)|_{TV(\hat{\Omega}_x)} \|\rho - \rho_\varepsilon\|_{L^1(\mathbb{R})}.$$

Now, we rewrite $f_\varepsilon(\beta) \circ^+ g_\varepsilon(\alpha)$ as a NN,

$$(B.12) \quad \begin{aligned} & f_\varepsilon(\beta) \circ^+ g_\varepsilon(\alpha)(x) \\ &= \sum_{k=1}^K \bar{c}_k(\beta) \rho_\varepsilon(x - g(\alpha)(x_k)) \\ &= \sum_{k=1}^K \bar{c}_k(\beta) \frac{1}{\varepsilon} \left[\sigma \left(x + \frac{\varepsilon}{2} - g(\alpha)(x_k) \right) - \sigma \left(x - \frac{\varepsilon}{2} - g(\alpha)(x_k) \right) \right], \end{aligned}$$

so one can write

$$(B.13) \quad f_\varepsilon(\beta) \circ^+ g_\varepsilon(\alpha)(x) = W^2 \sigma(W^1 x + B^1) + B^2, \quad x \in \Omega_x,$$

with the weights and biases

$$(B.14) \quad \begin{aligned} W^1 &= [1, 1, \dots, 1]^T \in \mathbb{R}^{2K \times 1}, \\ W^2 &= [\bar{c}_1(\beta), \bar{c}_1(\beta), \bar{c}_2(\beta), \bar{c}_2(\beta), \dots, \bar{c}_K(\beta), \bar{c}_K(\beta)] \in \mathbb{R}^{1 \times 2K}, \end{aligned}$$

$$\begin{aligned} B^1 &= \left[\frac{\varepsilon}{2} - g(\alpha)(x_1), -\frac{\varepsilon}{2} - g(\alpha)(x_1), \dots, \frac{\varepsilon}{2} - g(\alpha)(x_K), -\frac{\varepsilon}{2} - g(\alpha)(x_K) \right]^T \in \mathbb{R}^{2K \times 1}, \\ B^2 &= 0 \in \mathbb{R}^{1 \times 1}. \end{aligned}$$

We reorganize the NNs as 2-layer LRNR H_r in the form (4.16) in Exmpl. 4.4. Let $\{e_i\}_{i=1}^r$ denote the standard basis of \mathbb{R}^r . We write the weights W^1, W^2 as

$$(B.15) \quad W^1 = e_1 \cdot \mathbb{U}_r^1, \quad W^2 = [\beta_1, \dots, \beta_{r-1}, 0] \cdot \mathbb{U}_r^2,$$

where $\mathbb{U}_r^1 \subset \mathbb{R}^{2K \times 1}$ and $\mathbb{U}_r^2 \subset \mathbb{R}^{1 \times 2K}$ are given by

$$(B.16) \quad \begin{aligned} \mathbb{U}_r^1 &= (U_i^1)_{i=1}^r, \quad [U_i^1]_j := 1, \text{ for all } i, j, \\ \mathbb{U}_r^2 &= (U_i^2)_{i=1}^r, \quad \begin{cases} [U_i^2]_j := \bar{c}_{\lfloor j/2 \rfloor}(e_i) & \text{for } i = 1, \dots, r-1 \\ [U_i^2]_j := 0 & \text{for } i = r. \end{cases} \end{aligned}$$

Write the biases B^1, B^2 as

$$(B.17) \quad B^1 = [\alpha_1, \alpha_2, \dots, \alpha_{r-1}, 1] \cdot \mathbb{V}_r^1, \quad B^2 = 0 \cdot \mathbb{V}_r^2,$$

where $\mathbb{V}_r^1 \subset \mathbb{R}^{2K \times 1}$ and $\mathbb{V}_r^2 \subset \mathbb{R}^{1 \times 1}$ are defined by

$$(B.18) \quad \begin{aligned} \mathbb{V}_r^1 &= (V_i^1)_{i=1}^r, \quad \begin{cases} [V_i^1]_j := \psi_i(x_{\lfloor j/2 \rfloor}) & \text{for } i = 1, \dots, r-1 \\ [V_i^1]_j := 0 & \text{for } i = r, \end{cases} \\ \mathbb{V}_r^2 &= (V_i^2)_{i=1}^r, \quad V_i^2 := 0, \quad \text{for all } i. \end{aligned}$$

Defining the map μ over $A \times B$, whose mapped values $\mu(\alpha, \beta) = (\gamma, \theta)$ have individual entries $\gamma = (\gamma^1, \gamma^2)$ and $\theta = (\theta^1, \theta^2)$ that are given by

$$(B.19) \quad \begin{aligned} \gamma^1 &= e_1, & \gamma^2 &= [\beta_1, \dots, \beta_{r-1}, 0]^T, \\ \theta^1 &= [\alpha_1, \dots, \alpha_{r-1}, 1]^T, & \theta^2 &= 0, \end{aligned}$$

the LRNR $h(\gamma, \theta)$ is defined as in Exmpl. 4.4 with the coefficients (B.19) and weights and biases (B.15-B.17). By construction, it satisfies

$$(B.20) \quad h(\gamma, \theta) = f_\varepsilon(\beta) \circ^+ g_\varepsilon(\alpha).$$

Plugging (B.20) into (B.11),

$$(B.21) \quad \|f(\beta) \circ g(\alpha)^+ - h(\gamma, \theta)\|_{L^1(\Omega_x)} \leq |f(\beta)|_{TV(\hat{\Omega}_x)} \|\rho - \rho_\varepsilon\|_{L^1(\mathbb{R})}.$$

The desired inequality follows from

$$(B.22) \quad |f(\beta)|_{TV(\hat{\Omega}_x)} \leq \left| \sum_i \beta_i \psi_i \right|_{TV(\hat{\Omega}_x)} \leq \max_i |\beta_i| \sum_i |\psi_i|_{TV(\hat{\Omega}_x)}.$$

B.4 Proof of Lemma 5.1 By construction we have for any $t_k \in \Omega_t$

$$(B.23) \quad \hat{X}(\cdot, t_k) = \Xi_k(\cdot, t_k),$$

and for $t \in [t_k, t_{k+1}]$

$$(B.24) \quad \hat{X}(z, t) = \Xi_k(z, t) \quad \text{for all } z \in \hat{\Omega}_x \setminus \Upsilon_t.$$

Let us fix $x_0 \in \Upsilon_{t_k}$ and recall \hat{X}_0 is the rarefied characteristics with multivalued inverse (2.26). Then we have

$$(B.25) \quad \begin{aligned} E_k(t; x_0) &:= \sup_{x \in [\vdash(x_0, t), \dashv(x_0, t)]} \|\hat{X}(x, t) - \Xi_k(x, t)\| \\ &\leq \int_{t_k}^t \sup_{\substack{z \in [\vdash(x_0, t), \vdash(x_0, t_k)] \\ w \in [\dashv(x_0, t_k), \dashv(x_0, t)]}} \left| \frac{\partial \hat{X}_0}{\partial t}(z, t) - \frac{\partial \hat{X}_0}{\partial t}(w, t) \right| d\tau \\ &\leq \left(\sup_{\substack{z \in [\vdash(x_0, t), \vdash(x_0, t_k)] \\ w \in [\dashv(x_0, t_k), \dashv(x_0, t)]}} |(F' \circ \hat{u}_0)(z) - (F' \circ \hat{u}_0)(w)| \right) \cdot |t - t_k| \\ &\leq \|F''\|_{L^\infty([\underline{u}_{\text{loc}}, \bar{u}_{\text{loc}}])} (\bar{u}_{\text{loc}} - \underline{u}_{\text{loc}}) \cdot |t - t_k|, \end{aligned}$$

where we let

$$(B.26) \quad \begin{aligned} \bar{u}_{\text{loc}} &:= \sup_{\substack{z \in [\vdash(x_0, t), \vdash(x_0, t_k)] \\ \cup [\dashv(x_0, t_k), \dashv(x_0, t)]}} u_0(z), \\ \underline{u}_{\text{loc}} &:= \inf_{\substack{z \in [\vdash(x_0, t), \vdash(x_0, t_k)] \\ \cup [\dashv(x_0, t_k), \dashv(x_0, t)]}} u_0(z). \end{aligned}$$

Since $[\bar{u}_{\text{loc}}, \underline{u}_{\text{loc}}] \subset u_0(\Omega_x)$, we obtain the first estimate (5.14).

Next, we prove the second upper bound. By construction $\Xi_k(\cdot, t)$ equals $\hat{X}_0(\cdot, t)$ within Υ_{t_k} so we have

$$(B.27) \quad \begin{aligned} |\Xi_k(\cdot, t)|_{TV(\hat{\Omega}_x)} &\leq |\Xi_k(\cdot, t)|_{TV(\Upsilon_{t_k})} + |\Xi_k(\cdot, t)|_{TV(\hat{\Omega}_x \setminus \Upsilon_{t_k})} \\ &\leq |\Xi_k(\cdot, t)|_{TV(\Upsilon_{t_k})} + |\hat{X}_0(\cdot, t)|_{TV(\hat{\Omega}_x \setminus \Upsilon_{t_k})}. \end{aligned}$$

To estimate the first term on the RHS, note that $\Xi_k(\cdot, t)$ restricted to Υ_{t_k} is a linear interpolant of $\hat{X}_0(\cdot, t)$. More specifically, for any $x_0 \in \Upsilon_{t_k}$,

$$(B.28) \quad \begin{aligned} |\Xi_k(\cdot, t)|_{TV([\vdash(x_0, t_k), \dashv(x_0, t_k)])} &= \left| \hat{X}_0(\vdash(x_0, t_k), t) - \hat{X}_0(\dashv(x_0, t_k), t) \right| \\ &\leq |\hat{X}_0(\cdot, t)|_{TV([\vdash(x_0, t_k), \dashv(x_0, t_k)])}, \end{aligned}$$

and the local total variation bound is then naturally extended to Υ_{t_k} ,

$$(B.29) \quad |\Xi_k(\cdot, t)|_{TV(\Upsilon_{t_k})} \leq |\hat{X}_0(\cdot, t)|_{TV(\Upsilon_{t_k})}.$$

Using this in (B.27), we have that

$$(B.30) \quad \begin{aligned} |\Xi_k(\cdot, t)|_{TV(\hat{\Omega}_x)} &\leq |\hat{X}_0(\cdot, t)|_{TV(\hat{\Omega}_x)} = |\hat{I} + tF' \circ \hat{u}_0|_{TV(\hat{\Omega}_x)} \\ &\leq |\Omega_x| + T|u_0|_{TV(\Omega_x)} \|F''\|_{L^\infty(u_0(\Omega_x))}, \end{aligned}$$

which is the desired inequality upon inserting $|\Omega_x| = 1$.

B.4.1 Remark Note that the upper bound (5.14) with the TV norm $|u_0|_{TV(\Omega_x)}$ obtained from the last term in (B.25) is not sharp, and can be replaced by $2\|u_0\|_{L^\infty(\Omega_x)}$ because $|\bar{u}_{\text{loc}} - \underline{u}_{\text{loc}}| \leq 2\|u_0\|_{L^\infty([\vdash(x_0, t), \dashv(x_0, t)])}$, but we will keep the TV norm here, as doing so this will not affect the final results of this work.

B.5 Proof of Theorem 4.6 We write the classical solution $u(t) = u(\cdot, t)$ as

$$(B.31) \quad \begin{aligned} u(\cdot, t) &= u_0 \circ X^{-1}(\cdot, t) \\ &= u_0 \circ (\text{Id}(\cdot) + t(F' \circ u_0)(\cdot))^{-1}, \end{aligned}$$

then it is clear that the set of solutions forms a transported subspace, so Thm. 4.5 applies. Recall that the approximation proceeds below: Letting $\hat{\Omega}_x = \Omega_x$, define $u_{0\varepsilon}, X_\varepsilon \in C(\Omega_x) \cap P_1(\Omega_x)$ for which Lem. 4.3 implies

$$(B.32) \quad \begin{aligned} &\|u_0 \circ X^+ - u_{0\varepsilon} \circ^+ X_\varepsilon\|_{L^1(\Omega_x)} \\ &\leq \|X'\|_{L^\infty(\Omega_x)} \|u_0 - u_{0\varepsilon}\|_{L^1(\Omega_x)} \\ &\quad + |u_0|_{TV(\Omega_x)} \left((1 + \|X'\|_{L^\infty(\Omega_x)}) \|\rho - \rho_\varepsilon\|_{L^1(\mathbb{R})} + \|X - X_\varepsilon\|_{L^\infty(\mathcal{X})} \right), \end{aligned}$$

then picking X_ε so that it interpolates X at the points in $\mathcal{X} \subset \Omega_x$ as set in Lem. 4.3, the norm $\|X - X_\varepsilon\|_{L^\infty(\mathcal{X})} = 0$, so we have

$$(B.33) \quad \begin{aligned} &\|u_0 \circ X^+ - u_{0\varepsilon} \circ^+ X_\varepsilon\|_{L^1(\Omega_x)} \\ &\leq \|X'\|_{L^\infty(\Omega_x)} \|u_0 - u_{0\varepsilon}\|_{L^1(\Omega_x)} + |u_0|_{TV(\Omega_x)} (1 + \|X'\|_{L^\infty(\Omega_x)}) \|\rho - \rho_\varepsilon\|_{L^1(\mathbb{R})}. \end{aligned}$$

As shown in (B.20) in the proof of Thm. 4.5, there is a LRNR h satisfying

$$(B.34) \quad \begin{aligned} &\|u_{0\varepsilon} \circ^+ X_\varepsilon(t) - h(t)\|_{L^1(\Omega_x)} \\ &\leq T|u_0|_{TV(\Omega_x)} \|\rho - \rho_\varepsilon\|_{L^1(\mathbb{R})} + \frac{1}{K} \|X'\|_{L^\infty(\Omega_x)} |u_0|_{TV(\Omega_x)}, \end{aligned}$$

due to the estimate

$$(B.35) \quad \|X'\|_{L^\infty(\Omega_x)} \leq 1 + T\|F''\|_{L^\infty(u_0(\Omega_x))} \|u'\|_{L^\infty(\Omega_x)}.$$

Setting ε to be sufficiently small, the result follows by (B.33) and (B.34).

The coefficients γ, θ are induced by the mapping μ given by Thm. 4.5, see (B.19). The transported subspace coefficients depend linearly on t or are constant respect to it, thus γ, θ are linear or constant functions of t .

B.6 Proof of Theorem 5.2 By construction, $\bar{\pi}(\cdot, t)$ is based on $\eta_k \in C(\hat{\Omega}_x) \cap P_1(\hat{\Omega}_x)$ given in (5.21) for index $k = 1, \dots, K-1$ in (5.25) so we have for $t \in [t_k, t_{k+1}]$

$$\begin{aligned}
& \left\| \hat{X}(\cdot, t) - \bar{\pi}(\cdot, t) \right\|_{L^\infty(\hat{\Omega}_x)} \\
& \leq \left\| \pi(\cdot, t) - \bar{\pi}(\cdot, t) \right\|_{L^\infty(\hat{\Omega}_x)} + \left\| \hat{X}(\cdot, t) - \pi(\cdot, t) \right\|_{L^\infty(\hat{\Omega}_x)} \\
& \leq \|t\eta_k\|_{L^\infty(\hat{\Omega}_x)} + \left\| \hat{X}(\cdot, t) - \pi(\cdot, t) \right\|_{L^\infty(\hat{\Omega}_x)} \\
& \leq \frac{4C_{u_0, T, F}}{K} + \frac{1 + 6C_{u_0, T, F}}{K} \leq \frac{1 + 10C_{u_0, T, F}}{K},
\end{aligned} \tag{B.36}$$

upon applying (5.22) and (5.24). The RHS does not depend on the interval $[t_k, t_{k+1}]$ that t belongs to, so the result follows.

B.7 Proof of Theorem 5.3 We initially suppose $u_0 \in \bar{\mathcal{U}}$ so that $u_0 = \bar{u}_0$. We begin by providing an upper bound on the derivative of \hat{X} . Recall that \hat{X} is continuous and piecewise smooth, therefore its weak derivative \hat{X}' is in $L^\infty(\hat{\Omega}_x)$. Decomposing the extended domain into the shock set Υ_t and its complement

$$\hat{\Omega}_x = (\hat{\Omega}_x \setminus \Upsilon_t) \cup \Upsilon_t, \tag{B.37}$$

we have that \hat{X} is constant in Υ_t so that $\|\hat{X}'\|_{L^\infty(\Upsilon_t)} = 0$. Now recall the intervals inserted into in the extended domain $\Gamma_x = \bigcup_{k=1}^{n_R} \Gamma_k$ defined in (2.18). Writing the shock-free part of the extended domain $\hat{\Omega}_x \setminus \Upsilon_t$ into Γ_x and its complement

$$\hat{\Omega}_x \setminus \Upsilon_t = \left((\hat{\Omega}_x \setminus \Upsilon_t) \setminus \Gamma_x \right) \cup \Gamma_x, \tag{B.38}$$

we straightforwardly bound,

$$\begin{aligned}
\|\hat{X}'\|_{L^\infty(\hat{\Omega}_x)} & \leq \|\hat{X}'\|_{L^\infty(\hat{\Omega}_x \setminus \Upsilon_t)} + \|\hat{X}'\|_{L^\infty(\Upsilon_t)} \\
& \leq \|\hat{X}'\|_{L^\infty((\hat{\Omega}_x \setminus \Upsilon_t) \setminus \Gamma_x) \cup (\Gamma_x \setminus \Upsilon_t))} \\
& \leq 1 + T \max \left\{ \|(F' \circ \hat{u}_0)'\|_{L^\infty((\hat{\Omega}_x \setminus \Upsilon_t) \setminus \Gamma_x)}, \|(F' \circ \hat{u}_0)'\|_{L^\infty(\Gamma_x)} \right\}.
\end{aligned} \tag{B.39}$$

Due to the way of \hat{u}_0 was defined in (2.20), for $k = 1, \dots, n_R$,

$$\begin{aligned}
\|(F' \circ \hat{u}_0)'\|_{L^\infty(\Gamma_k)} & = \left\| \nu_k^- + \frac{\nu_k^+ - \nu_k^-}{\varepsilon_k} (\cdot - \iota(\xi_k)) \right\|_{L^\infty(\iota(\xi_k) + [0, \varepsilon_k))} \\
& = \max_{\pm} |\nu_k^{\pm}| \leq \|(F' \circ u_0)'\|_{L^\infty(\Omega_x)},
\end{aligned} \tag{B.40}$$

since the L^∞ -norm is taken over a linear function connecting ν_k^- and ν_k^+ . So we obtain the L^∞ estimate

$$\|\hat{X}'\|_{L^\infty(\hat{\Omega}_x)} \leq 1 + T \|(F' \circ u_0)'\|_{L^\infty(\Omega_x)} \leq 1 + T \|F''\|_{L^\infty(u_0(\Omega_x))} |u_0|_{TV(\Omega_x)}, \tag{B.41}$$

which is a generalization of the crude bound (B.35) for classical characteristics.

Due to Lem. 4.3, and choosing $\epsilon = 1/K$ so that $\|\rho - \rho_\varepsilon\|_{L^1(\mathbb{R})} \lesssim 1/K$ we have

$$\begin{aligned}
& \|u(\cdot, t) - \bar{h}(\cdot, t)\|_{L^1(\Omega_x)} \\
& \leq \|\hat{X}'\|_{L^\infty(\hat{\Omega}_x)} \|\hat{u}_0 - \hat{u}_{0\varepsilon}\|_{L^1(\hat{\Omega}_x)} \\
& \quad + |u_0|_{TV(\Omega_x)} \left(\left(1 + \|\hat{X}'\|_{L^\infty(\hat{\Omega}_x)} \right) \|\rho - \rho_\varepsilon\|_{L^1(\mathbb{R})} + \|\hat{X} - \bar{\pi}\|_{L^1(\mathbb{R})} \right).
\end{aligned} \tag{B.42}$$

The result follows from the estimates (5.27) and (B.41), and further,

$$(B.43) \quad \|u(\cdot, t) - \bar{h}(\cdot, t)\|_{L^1(\Omega_x)} \lesssim \frac{1}{K} |u_0|_{TV} + \frac{1}{K} |u_0|_{TV}^2 T \|F''\|_{L^\infty(u_0(\Omega_x))}.$$

Gathering the terms,

$$(B.44) \quad \begin{aligned} & \|u(\cdot, t) - \bar{h}(\cdot, t)\|_{L^1(\Omega_x)} \\ & \lesssim \frac{1}{K} |u_0|_{TV} (1 + |u_0|_{TV}) (1 + T \|F''\|_{L^\infty(u_0(\Omega_x))}). \end{aligned}$$

Finally, lifting the restriction that $u_0 \in \bar{\mathcal{U}}$, then employing a density argument followed by an application of the triangle inequality, the desired estimate is obtained.

B.8 Proof of Theorem 5.4 Each solution to the IVP with $u_0 \in \mathcal{U}$ can be uniformly approximated by one with $\bar{u}_0 \in \bar{\mathcal{U}}$, so it suffices to consider that case. Recall the approximation of the initial data of the form $\hat{u}_{0\varepsilon}$ (5.29) with its grid $(x_i)_{i=1}^K$ and coefficients $(\hat{u}_{0,i})_{i=1}^K$, along with the approximation $\bar{\pi}$ (5.25) of the rarefied characteristics.

We will show that the piecewise approximation $h(x, t)$ (5.31) can be represented by a LRNR. Denote the hidden variables by

$$(B.45) \quad Z^{\ell+1} = W^\ell \sigma(Z^\ell) + B^\ell, \quad \ell = 0, \dots, L-1,$$

and the initial input is $Z^0 := x$. We remind the reader that in our setting, the spatial variable x is the sole input to the NN, and the time variable t is an external parameter. We use the notation $[N] := \{1, 2, \dots, N\}$ for $N \in \mathbb{N}$ and the Einstein summation convention for the subscripts. We will use higher-dimensional tensors to specify the hidden variables and the affine mappings instead of using vectors and matrices, in order to simplify the index notation.

We construct the first layer ($\ell = 1$) so that we have

$$(B.46) \quad \mathbb{R}^{K \times 3 \times K} \ni Z_{ijk}^1 = \begin{cases} x, & i \in [K], j = k = 1, \\ x_i, & i \in [K], j = 2, k = 1, \\ t - t_k, & i = 1, j = 3, k \in [K], \\ 0, & \text{otherwise.} \end{cases}$$

Note also that only $\sim K$ entries are non-zero. We obtain this by

$$(B.47) \quad W_{ijk}^1 = \begin{cases} 1, & j, k = 1, i \in [K], \\ 0, & \text{otherwise,} \end{cases}$$

and

$$(B.48) \quad B_{ijk}^1 = \begin{cases} x_i, & i \in [K], j = 2, k = 1, \\ t - t_k, & i = 1, j = 3, k \in [K], \\ 0, & \text{otherwise,} \end{cases}$$

B here has linear or constant dependence on t of rank two.

We construct the second layer ($\ell = 2$) so that we have

$$(B.49) \quad \mathbb{R}^{K \times K \times 2} \ni Z_{pqn}^2 = \begin{cases} x, & n = q = 1, p \in [K], \\ x_p - z_q - \sigma \left(\frac{1}{\varepsilon_0} (t - t_q) \right), & n = 2, p, q \in [K], \\ 0, & \text{otherwise,} \end{cases}$$

with $\varepsilon_0 := T/K$, and recall that $(z_k)_{k=1}^K$ is the adaptive grid used for constructing Ξ_k (5.12). We obtain this by assigning the weights

$$(B.50) \quad W_{ijk,pqn}^2 = \begin{cases} \delta_{ip}, & s = 1, j = 1, i, p \in [K], n = 1, \\ \delta_{ip}, & s = 2, j = 2, i \in [K], n \in [K], \\ -\frac{\delta_{kq}}{\varepsilon_0}, & s = 2, i = 1, j = 3, k, q \in [K], \\ 0, & \text{otherwise,} \end{cases}$$

and the bias

$$(B.51) \quad B_{pqn}^2 = \begin{cases} -z_q, & n = 2, p \in [K], q \in [K], \\ 0, & \text{otherwise,} \end{cases}$$

and recalling that $\sigma(z)/\varepsilon_0 = \sigma(z/\varepsilon_0)$. This layer has rank one, and the operations are identical for each p in this and the subsequent layer, so it is parallelizable.

We construct the third layer ($\ell = 3$) so that we have

$$(B.52) \quad \mathbb{R}^{K \times 2} \ni Z_{ij}^3 = \begin{cases} x, & i \in [K], j = 1, \\ x_i + \bar{\pi}(x_i, t), & i \in [K], j = 2, \\ 0, & \text{otherwise,} \end{cases}$$

We obtain this by setting

$$(B.53) \quad W_{ij,pqn}^3 = \begin{cases} \delta_{ip}, & n = q = j = 1, i, p \in [K], \\ a_q(t) \delta_{ip}, & j = n = 2, i, p \in [K], \\ 0, & \text{otherwise,} \end{cases}$$

and

$$(B.54) \quad B_{ij}^3 = \begin{cases} 0, & j = 1, \\ \bar{\pi}_K(x_i, t), & i \in [K], j = 2, \\ 0, & \text{otherwise,} \end{cases}$$

in which we set the coefficients $a_q(t)$, an linear or constant function of t , to obtain the the function (5.25) of above. This layer has rank two.

We construct the fourth layer ($\ell = 4$) so that we have

$$(B.55) \quad \mathbb{R}^{K \times 2} \ni Z_{ps}^4 = \begin{cases} \sigma \left(-\frac{1}{\varepsilon_1} (x - x_p - \bar{\pi}(x_p, t)) - \frac{1}{2} \right), & p \in [K], s = 1, \\ \sigma \left(\frac{1}{\varepsilon_1} (x - x_p - \bar{\pi}(x_p, t)) + \frac{1}{2} \right), & p \in [K], s = 2, \\ 0, & \text{otherwise,} \end{cases}$$

where we set $\varepsilon_1 < \min_{p,q \in [K], p \neq q} |x_p - x_q|$. We obtain this by setting

$$(B.56) \quad W_{ps,ij}^4 = \begin{cases} \frac{(-1)^{(j+s+1)}}{\varepsilon_1} \delta_{pi}, & s = 1, 2, i, p \in [K], j = 1, 2, \\ 0, & \text{otherwise,} \end{cases}$$

and

$$(B.57) \quad B_{ps}^4 = (-1)^{(s+1)}/2, \quad s = 1, 2, p \in [K].$$

The layer has rank one.

We construct the fifth layer ($\ell = 5$) so that we have

$$(B.58) \quad h(x, t) = \sum_{j=1}^K \hat{u}_{0,j} \rho_\varepsilon(x - \bar{\pi}(x_j, t)).$$

We assign the weights that approximate the extended initial condition \hat{u}_0 ,

$$(B.59) \quad W_{ps}^5 = (-1)^{s+1} \hat{u}_{0,p}, \quad s = 1, 2, \quad p \in [K],$$

and then let B^5 be zero. These weights take linear combinations of the inputs from the previous layer Z^4 (B.55) so that $\rho_\varepsilon(x - \bar{\pi}(x_j, t))$ is computed; note how ρ_ε was written as a sum of two ReLUs (4.9). The layer has rank one.

Then we have that $h(x, t)$ is equal to $\bar{h}(x, t)$, so the error estimate follows from that for \bar{h} (Thm. 5.3). All the weights and biases can be written as a linear combination of at most two basis elements, and the coefficients are either constant or linear with respect to t .

REFERENCES

- [1] R. ABGRALL, D. AMSALEM, AND R. CRISOVAN, *Robust model reduction by L^1 -norm minimization and approximation via dictionaries: Application to linear and nonlinear hyperbolic problems*, Advanced Modeling and Simulation in Engineering Sciences, 3 (2016), p. 1.
- [2] J. BARNETT, C. FARHAT, AND Y. MADAY, *Neural-network-augmented projection-based model order reduction for mitigating the Kolmogorov barrier to reducibility*, Journal of Computational Physics, 492 (2023), p. 112420.
- [3] J. BERNER, P. GROHS, G. KUTYNIOK, AND P. PETERSEN, *The Modern Mathematics of Deep Learning*, Cambridge University Press, Cambridge, UK, 2022.
- [4] W. J. BEYN AND V. THÜMMLER, *Freezing Solutions of Equivariant Evolution Equations*, SIAM Journal on Applied Dynamical Systems, 3 (2004), pp. 85–116.
- [5] H. BÖLCSKEI, P. GROHS, G. KUTYNIOK, AND P. PETERSEN, *Optimal Approximation with Sparsely Connected Deep Neural Networks*, SIAM Journal on Mathematics of Data Science, 1 (2019), pp. 8–45.
- [6] F. BOLLEY, Y. BRENIER, AND G. LOEPER, *Contractive metrics for scalar conservation laws*, Journal of Hyperbolic Differential Equations, 02 (2005), pp. 91–107.
- [7] N. BONNEEL, J. RABIN, G. PEYRÉ, AND H. PFISTER, *Sliced and Radon Wasserstein barycenters of measures*, Journal of Mathematical Imaging and Vision, 51 (2015), pp. 22–45.
- [8] Y. BRENIER, *Averaged Multivalued Solutions for Scalar Conservation Laws*, SIAM Journal on Numerical Analysis, 21 (1984), pp. 1013–1037.
- [9] N. CAGNIART, Y. MADAY, AND B. STAMM, *Model Order Reduction for Problems with Large Convection Effects*, Springer International Publishing, Cham, Switzerland, 2019, pp. 131–150.
- [10] S. CAI, Z. MAO, Z. WANG, M. YIN, AND G. E. KARNIADAKIS, *Physics-informed neural networks (pinns) for fluid mechanics: a review*, Acta Mechanica Sinica, 37 (2021), pp. 1727–1738.

[11] CARROLL AND DICKINSON, *Construction of neural nets using the radon transform*, in International 1989 Joint Conference on Neural Networks, 1989, pp. 607–611 vol.1.

[12] W. CHO, K. LEE, N. PARK, D. RIM, AND G. WELPER, *FastLRNR and Sparse Physics Informed Backpropagation*, Results in Applied Mathematics, 25 (2025), p. 100547.

[13] W. CHO, K. LEE, D. RIM, AND N. PARK, *Hypernetwork-based meta-learning for low-rank physics-informed neural networks*, in Advances in Neural Information Processing Systems, vol. 36, Red Hook, NY, 2023, Curran Associates, Inc., pp. 11219–11231.

[14] A. COHEN AND R. DEVORE, *Approximation of high-dimensional parametric PDEs*, Acta Numerica, 24 (2015), pp. 1–159.

[15] A. COHEN, R. DEVORE, G. PETROVA, AND P. WOJTASZCZYK, *Optimal stable nonlinear approximation*, Foundations of Computational Mathematics, 22 (2022), pp. 607–648.

[16] P. G. CONSTANTINE AND G. IACCARINO, *Reduced order models for parameterized hyperbolic conservations laws with shock reconstruction*, Center for Turbulence Research Annual Brief, (2012).

[17] S. CUOMO, V. S. DI COLA, F. GIAMPAOLO, G. ROZZA, M. RAISI, AND F. PICCIALLI, *Scientific machine learning through physics-informed neural networks: Where we are and what's next*, Journal of Scientific Computing, 92 (2022), p. 88.

[18] C. M. DAFLEROS, *Polygonal approximations of solutions of the initial value problem for a conservation law*, Journal of Mathematical Analysis and Applications, 38 (1972), pp. 33–41.

[19] C. M. DAFLEROS, *Hyperbolic Conservation Laws in Continuum Physics*, Springer Berlin Heidelberg, Berlin, Heidelberg, 2010.

[20] W. DAHMEN, *Compositional Sparsity, Approximation Classes, and Parametric Transport Equations*, (2023), [arXiv:2207.06128](https://arxiv.org/abs/2207.06128).

[21] W. DAHMEN, C. PLESKEN, AND G. WELPER, *Double greedy algorithms: Reduced basis methods for transport dominated problems*, ESAIM: Mathematical Modelling and Numerical Analysis, 48 (2014), pp. 623–663.

[22] R. DEVORE, B. HANIN, AND G. PETROVA, *Neural network approximation*, Acta Numerica, 30 (2021), pp. 327–444.

[23] R. A. DEVORE, *Nonlinear approximation*, Acta Numerica, 7 (1998), pp. 51–150.

[24] V. EHRLACHER, D. LOMBARDI, O. MULA, AND F.-X. VIALARD, *Nonlinear model reduction on metric spaces. Application to one-dimensional conservative PDEs in Wasserstein spaces*, ESAIM: Mathematical Modelling and Numerical Analysis, 54 (2020), pp. 2159–2197.

[25] S. FRESCA, L. DEDÉ, AND A. MANZONI, *A comprehensive deep learning-based approach to reduced order modeling of nonlinear time-dependent parametrized pdes*, Journal of Scientific Computing, 87 (2021), p. 61.

[26] R. GEELIN, S. WRIGHT, AND K. WILLCOX, *Operator inference for non-intrusive model reduction with quadratic manifolds*, Computer Methods in Applied Mechanics and Engineering, 403 (2023), p. 115717.

[27] M. GEIST, P. PETERSEN, M. RASLAN, R. SCHNEIDER, AND G. KUTYNIOK, *Numerical solution of the parametric diffusion equation by deep neural networks*, Journal of Scientific Computing, 88 (2021), p. 22.

[28] J.-F. GERBEAU AND D. LOMBARDI, *Approximated Lax pairs for the reduced order integration of nonlinear evolution equations*, Journal of Computational Physics, 265 (2014), pp. 246 – 269.

[29] F. J. GONZALEZ AND M. BALAJEWICZ, *Deep convolutional recurrent autoencoders for learning low-dimensional feature dynamics of fluid systems*, (2018), [arXiv:1808.01346](https://arxiv.org/abs/1808.01346).

[30] I. GOODFELLOW, Y. BENGIO, AND A. COURVILLE, *Deep Learning*, MIT Press, Cambridge, MA, 2016. <http://www.deeplearningbook.org>.

[31] C. GREIF AND K. URBAN, *Decay of the Kolmogorov N-width for wave problems*, Applied Mathematics Letters, 96 (2019), pp. 216 – 222.

[32] B. HAASDONK AND M. OHLBERGER, *Reduced basis method for finite volume approximations of parametrized linear evolution equations*, ESAIM: Mathematical Modelling and Numerical Analysis, 42 (2008), pp. 277–302.

[33] J. K. HALE, *Ordinary Differential Equations*, Wiley-Interscience, New York, 2nd ed., 1980.

[34] J. HAN, A. JENTZEN, AND E. WEINAN, *Solving high-dimensional partial differential equations using deep learning*, Proceedings of the National Academy of Sciences, 115 (2018), pp. 8505–8510.

[35] S. HELGASON, *Integral Geometry and Radon Transforms*, Springer New York, New York, NY,

2011.

- [36] J. HESTHAVEN AND S. UBBIALI, *Non-intrusive reduced order modeling of nonlinear problems using neural networks*, Journal of Computational Physics, 363 (2018), pp. 55–78.
- [37] J. S. HESTHAVEN, C. PAGLIANTINI, AND G. ROZZA, *Reduced basis methods for time-dependent problems*, Acta Numerica, 31 (2022), pp. 265–345.
- [38] J. S. HESTHAVEN, G. ROZZA, AND B. STAMM, *Certified Reduced Basis Methods for Parametrized Partial Differential Equations*, Springer, Cham, 2016.
- [39] H. HOLDEN AND N. H. RISEBRO, *Front Tracking for Hyperbolic Conservation Laws*, Springer Berlin Heidelberg, Berlin, Heidelberg, 2002.
- [40] A. IOLLO AND D. LOMBARDI, *Advection modes by optimal mass transfer*, Physical Review E, 89 (2014), p. 022923.
- [41] Y. KHOO, J. LU, AND L. YING, *Solving parametric PDE problems with artificial neural networks*, European Journal of Applied Mathematics, (2020), pp. 1–15.
- [42] Y. KIM, Y. CHOI, D. WIDEMANN, AND T. ZOHDI, *A fast and accurate physics-informed neural network reduced order model with shallow masked autoencoder*, Journal of Computational Physics, 451 (2022), p. 110841.
- [43] O. KOCH AND C. LUBICH, *Dynamical low-rank approximation*, SIAM Journal on Matrix Analysis and Applications, 29 (2007), pp. 434–454.
- [44] P. KRAH, S. BÜCHHOLZ, M. HÄRINGER, AND J. REISS, *Front transport reduction for complex moving fronts*, Journal of Scientific Computing, 96 (2023), p. 28.
- [45] A. KRISHNAPRIYAN, A. GHOLAMI, S. ZHE, R. KIRBY, AND M. W. MAHONEY, *Characterizing possible failure modes in physics-informed neural networks*, in Advances in Neural Information Processing Systems, vol. 34, Red Hook, NY, 2021, Curran Associates, Inc., pp. 26548–26560.
- [46] G. KUTYNIOK, P. PETERSEN, M. RASLAN, AND R. SCHNEIDER, *A Theoretical Analysis of Deep Neural Networks and Parametric PDEs*, Constructive Approximation, 55 (2022), pp. 73–125.
- [47] F. LAAKMANN AND P. PETERSEN, *Efficient approximation of solutions of parametric linear transport equations by ReLU DNNs*, Advances in Computational Mathematics, 47 (2021), p. 11.
- [48] K. LEE AND K. T. CARLBERG, *Model reduction of dynamical systems on nonlinear manifolds using deep convolutional autoencoders*, Journal of Computational Physics, 404 (2020), p. 108973.
- [49] R. J. LEVEQUE, *Large Time Step Shock-Capturing Techniques for Scalar Conservation Laws*, SIAM Journal on Numerical Analysis, 19 (1982), pp. 1091–1109.
- [50] R. J. LEVEQUE, *Finite Volume Methods for Hyperbolic Problems*, Cambridge Texts in Applied Mathematics, Cambridge University Press, Cambridge, UK, 2002.
- [51] R. J. LEVEQUE, *Finite Volume Methods for Hyperbolic Problems*, Cambridge University Press, Cambridge, 1st ed., 2002.
- [52] C. MARCATI, J. A. A. OPSCHOOR, P. C. PETERSEN, AND C. SCHWAB, *Exponential ReLU neural network approximation rates for point and edge singularities*, Foundations of Computational Mathematics, (2022), pp. 1615–3383.
- [53] A. T. MOHAN AND D. V. GAITONDE, *A deep learning based approach to reduced order modeling for turbulent flow control using lstm neural networks*, (2018), [arXiv:1804.09269](https://arxiv.org/abs/1804.09269).
- [54] R. MOJGANI AND M. BALAJEWICZ, *Lagrangian basis method for dimensionality reduction of convection dominated nonlinear flows*, (2017), [arXiv:1701.04343](https://arxiv.org/abs/1701.04343).
- [55] R. MOJGANI, M. BALAJEWICZ, AND P. HASSANZADEH, *Kolmogorov n -width and Lagrangian physics-informed neural networks: A causality-conforming manifold for convection-dominated PDEs*, Computer Methods in Applied Mechanics and Engineering, 404 (2023), p. 115810.
- [56] N. J. NAIR AND M. BALAJEWICZ, *Transported snapshot model order reduction approach for parametric, steady-state fluid flows containing parameter-dependent shocks*, International Journal for Numerical Methods in Engineering, 117 (2019), pp. 1234–1262.
- [57] F. NATTERER, *The Mathematics of Computerized Tomography*, Society for Industrial and Applied Mathematics, Philadelphia, PA, 2001.
- [58] N.-C. NGUYEN, G. ROZZA, AND A. T. PATERA, *Reduced basis approximation and a posteriori error estimation for the time-dependent viscous Burgers' equation*, Calcolo, 46 (2009), pp. 157–185.
- [59] M. OHLBERGER AND S. RAVE, *Nonlinear reduced basis approximation of parameterized evolution*

equations via the method of freezing, Comptes Rendus Mathematique, 351 (2013), pp. 901 – 906.

[60] M. OHLBERGER AND S. RAVE, *Reduced basis methods: Success, limitations and future challenges*, Proceedings of the Conference Algoritmy, (2016), pp. 1–12.

[61] G. ONGIE, R. WILLETT, D. SOUDRY, AND N. SREBRO, *A Function Space View of Bounded Norm Infinite Width ReLU Nets: The Multivariate Case*, in International Conference on Learning Representations, 2020.

[62] J. J. PARK, P. FLORENCE, J. STRAUB, R. NEWCOMBE, AND S. LOVEGROVE, *DeepSDF: Learning Continuous Signed Distance Functions for Shape Representation*, in Proceedings of the IEEE/CVF Conference on Computer Vision and Pattern Recognition (CVPR), June 2019.

[63] P. PETERSEN AND F. VOIGTLAENDER, *Optimal approximation of piecewise smooth functions using deep relu neural networks*, Neural Networks, 108 (2018), pp. 296–330.

[64] A. PINKUS, *n -Widths in Approximation Theory*, Springer, Berlin, Heidelberg, 1985.

[65] M. RAISSI, P. PERDIKARIS, AND G. KARNIADAKIS, *Physics-informed neural networks: A deep learning framework for solving forward and inverse problems involving nonlinear partial differential equations*, Journal of Computational Physics, 378 (2019), pp. 686–707.

[66] F. REGAZZONI, L. DEDÈ, AND A. QUATERONI, *Machine learning for fast and reliable solution of time-dependent differential equations*, Journal of Computational Physics, 397 (2019), p. 108852.

[67] J. REISS, P. SCHULZE, J. SESTERHENN, AND V. MEHRMANN, *The Shifted Proper Orthogonal Decomposition: A Mode Decomposition for Multiple Transport Phenomena*, SIAM Journal on Scientific Computing, 40 (2018), pp. A1322–A1344.

[68] D. RIM, *Dimensional splitting of hyperbolic partial differential equations using the Radon transform*, SIAM Journal on Scientific Computing, 40 (2018), pp. A4184–A4207.

[69] D. RIM AND K. MANDLI, *Displacement interpolation using monotone rearrangement*, SIAM/ASA Journal on Uncertainty Quantification, 6 (2018), pp. 1503–1531.

[70] D. RIM, S. MOE, AND R. LEVEQUE, *Transport Reversal for Model Reduction of Hyperbolic Partial Differential Equations*, SIAM/ASA Journal on Uncertainty Quantification, 6 (2018), pp. 118–150.

[71] D. RIM, B. PEHERSTORFER, AND K. T. MANDLI, *Manifold Approximations via Transported Subspaces: Model Reduction for Transport-Dominated Problems*, SIAM Journal on Scientific Computing, 45 (2023), pp. A170–A199.

[72] D. RIM, L. VENTURI, J. BRUNA, AND B. PEHERSTORFER, *Depth separation for reduced deep networks in nonlinear model reduction: Distilling shock waves in nonlinear hyperbolic problems*, (2020), [arXiv:2007.13977](https://arxiv.org/abs/2007.13977).

[73] D. RIM AND G. WELPER, *Performance bounds for Reduced Order Models with Application to Parametric Transport*, (2023), [arXiv:2310.14391](https://arxiv.org/abs/2310.14391).

[74] C. W. ROWLEY AND J. E. MARSDEN, *Reconstruction equations and the Karhunen-Loève expansion for systems with symmetry*, Physica D, (2000), pp. 1–19.

[75] T. P. SAPSIS AND P. F. LERMUSIAUX, *Dynamically orthogonal field equations for continuous stochastic dynamical systems*, Physica D: Nonlinear Phenomena, 238 (2009), pp. 2347–2360.

[76] D. SERRE, *Systems of Conservation Laws 1: Hyperbolicity, Entropies, Shock Waves*, Cambridge University Press, Cambridge, UK, 1999.

[77] V. SITZMANN, J. MARTEL, A. BERGMAN, D. LINDELL, AND G. WETZSTEIN, *Implicit Neural Representations with Periodic Activation Functions*, in Advances in Neural Information Processing Systems, vol. 33, Red Hook, NY, 2020, Curran Associates, Inc., pp. 7462–7473.

[78] T. TADDEI, *A Registration Method for Model Order Reduction: Data Compression and Geometry Reduction*, SIAM Journal on Scientific Computing, 42 (2020), pp. A997–A1027.

[79] TADDEI, TOMMASO AND ZHANG, LEI, *Space-time registration-based model reduction of parameterized one-dimensional hyperbolic PDEs*, ESAIM: Mathematical Modelling and Numerical Analysis, 55 (2021), pp. 99–130.

[80] I. TAYLOR, *The Korean writing system: An alphabet? A syllabary? a logography?*, Springer US, Boston, MA, 1980, pp. 67–82.

[81] M. UNSER, *Ridges, Neural Networks, and the Radon Transform*, Journal of Machine Learning Research, 24 (2023), pp. 1–33.

[82] Q. WANG, J. S. HESTHAVEN, AND D. RAY, *Non-intrusive reduced order modeling of unsteady flows using artificial neural networks with application to a combustion problem*, Journal of Computational Physics, 384 (2019), pp. 289–307.

- [83] G. Welper, *Interpolation of Functions with Parameter Dependent Jumps by Transformed Snapshots*, SIAM Journal on Scientific Computing, 39 (2017), pp. A1225–A1250.
- [84] D. YAROTSKY, *Error bounds for approximations with deep relu networks*, Neural Networks, 94 (2017), pp. 103–114.